Mimicking the Behaviors of Oil Contaminated Clays Using Functionalized Silica Nanoparticles

by

Xinci Huang

A thesis submitted in partial fulfillment of the requirements for the degree of

Master of Science

in

Chemical Engineering

Department of Chemical and Materials Engineering

University of Alberta

Abstract

Fine sand and clay particles arise naturally in diverse industrial and environmental remediation contexts. Organic compounds for example from oil production or oil spills can adsorb on their surface and influence their oil water interfacial behaviors. To isolate the impact of contamination and mimic contaminated clay behaviors, functionalized silica nanoparticles, with both aliphatic chains and aromatic group on their surface, were synthesized and their interfacial properties at oil-water interfaces were evaluated. The outcomes of this work shed light on the interfacial behaviors of contaminated clays in, for example, oil sands production processes. The interfacial tension between water and bare silica, silylated silica, silylated silica-octyl and silylated silica-anthracene nanoparticles suspension were measured. Factors that influence interfacial tension including nanoparticle concentration, pH and salinity (NaCl and $CaCl_2$) were investigated. While impacts of each of these variables is measurable, the overall impact of silica nanoparticle functionalization on interfacial behaviours is limited relative to bare silica, indicating that the interfacial behaviour of silica nanoparticles is dominated by the properties of the silica substrate. Functionalization does however impact nanoparticle aggregation. Silylated and silylated silica-octyl nanoparticles aggregate in toluene at high concentration.

Dedicated to

My parents and friends

Acknowledgements

First of all, I would like to express my deep gratitude to my supervisor Dr. Shaw, who gives me a lot of guidance and advice. His patience and optimism always got me of out the troubles I met during experiments. His brilliant thoughts have inspired me a lot to move forward and accomplish this work. I also want to thank Dr. Zeng for his timely advice and instruction. His experience was a great help with interfacial tension measurements and analysis.

I want to thank Mildred Becerra for her patience and assistance. Without her, I could not have carried out my experiments so smoothly. It's a great pleasure and luck working with such a lab manager.

I appreciate the help and suggestions of Amin Pourmohammadbagher. His guidance and patience have greatly helped me during my experiments. I also want to thank Shuo Zhang for the training on interfacial tension measurement. His experience and timely assistance really helped me to achieve data with higher quality. His knowledge also helped me better understand the interfacial properties I observed.

I would like to thank all my family members especially my parents for their unconditional love, support and encouragement. Without them, I could never have achieved what I have today.

Last but not least, I want to thank all the sponsors for their financial support. The Natural Sciences and Engineering Research Council Industrial Research Chair in Petroleum Thermodynamics (Alberta Innovates - Energy and Environment Solutions, BP Canada Energy Corporation, ConocoPhillips Canada Resource Corporation, Natural Sciences and Engineering Research Council of Canada (NSERC), Nexen Energy ULC, Shell Canada, Total E & P Canada, Virtual Materials Group Incorporated) is also gratefully acknowledged.

Table of Contents

List of Tables

List of Figures

CHAPTER 1: INTRODUCTION

Oil sands are is an important hydrocarbon energy resource and a driver economic of the Alberta economy. Even though the industry is mature, there are unresolved environmental problems related to oil sands production and processing. For mined oil sands, tailing ponds take up huge areas of land. As tailings separation from water is not adequately understood, land reclamation has been limited and the area required for tailings ponds has continued to grow. The current surface area of oil sands related tailings ponds in Alberta exceeds 100,000 km^2.[1]

Mined bitumen production begins with overburden removal and surface mining of oil sands. The mined oil sand is then crushed and mixed with water, and process chemicals to form a slurry.[2] For hot water based oil sands extraction, the temperature of the water is usually between 75°C to 80°C.[2] The slurry is conditioned in a tumbler and then fed to a froth flotation process where bitumen is liberated from the sand and separated. The bitumen is then fed into an upgrading process. Waste-water, sand and clay are transported by pipeline and then fed to a tailings pond. Figure 1.1 shows a simplified schematic of the oil sands production process. To extract one ton of bitumen from oil sands, 0.4 ton of water is needed. About 85% of process water is recycled. The water that cannot be recycled remains in the tailings pond or evaporates.

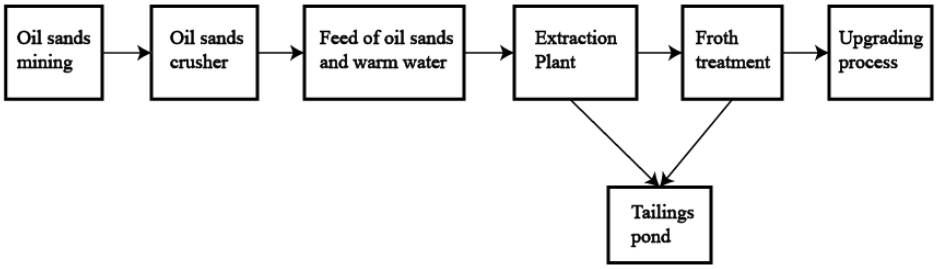

Figure 1.1 Oil sands production schematic.[2]

Following oil sands extraction, inorganic and organic chemical wastes, fine sand and clays that are dispersed or soluble in water are fed as slurry to tailings ponds.[3]Water-soluble constituents, such as naphthenic acids, are toxic to animals in water.[4] Oil slicks on tailings pond surfaces coat and kill birds. Even with a shift away from mining to in situ production methods that are largely waste water free, tailings ponds will continue to be hard to manage and will remain a legacy issue into the future.

To remediate and reclaim the land taken up by tailings ponds and reduce the impact of the pollution caused by tailings, one important step is to accelerate the settlement and compaction of sands and clays suspended in the waste slurry stream. Particle size varies from nanometers to micrometers. Their surface and other properties are also varied. These clays and sand particles are also contaminated by oil and weathered oil products arising evaporation of waste oil, or from direct oxidation, bacterial action over time. Water chemistry and in particular the interaction of water chemistry with particle chemistry also impacts settling rates.[5]The numbers of variables and their spatial and time

variation make the separation and settling process complex and have led to the difficulty of resolving this important environmental issue.

1.1 Tailings

Tailings comprise residual oil, waste water, minerals, metals, sands and clays, and also many other chemicals. Usually there are 20 wt. % to 30 wt. % of solids, the rest is waste water and a very small amount of oil (less than 3 wt. %).[6]The components are quite complicated and their percentages vary in different tailings ponds. Tailing ponds are the simplest and cheapest way to contain if not deal with this waste. Figure 1.2 shows the appearance of a tailings pond inlet section.

Figure 1.2 Picture of a tailings pond.[7]

Even though the components vary in different tailings ponds, tailings ponds have a similar structure as illustrated in Figure 1.3. The top layer of a tailing pond comprises recyclable water, with almost no solids and is ready to use for processing process in production. Underneath this layer, is the fluid fine tailings (FFT).[3]In this layer, there are finer sized clay particles, but the solid content is usually lower than the mature fine tailings (MFT), layer just beneath. Mature fine tailings contain more than 25 wt% of solids.[6] Because clays can stay in stable suspension for decades,[8] it is difficult to recover water trapped in this layer.

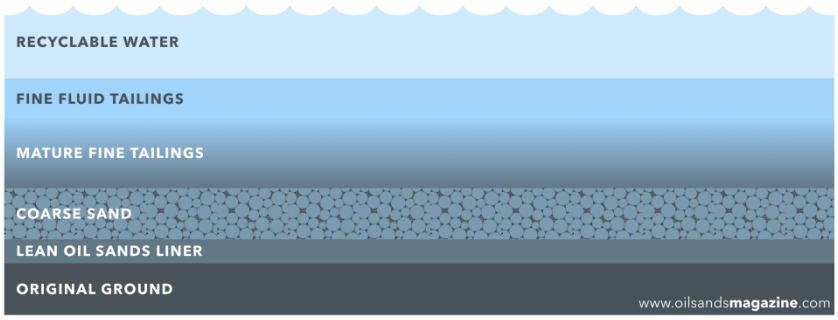

Figure 1.3 Cross-section of a tailing pond.[7]

1.2 Clay Minerals

Clay is one of the most troublesome constituents in tailings ponds and mature fine tailings that contain plenty of finer sized particles, which may take the longest time to solidify.[8] Clay particles are composed of sheets of silicon-oxygen tetrahedra and sheets of aluminum-or magnesium-oxygen octahedral.[9] Different types of clays have different arrangements of these sheets as their unit layer.[9] Depending on their structure, clay

minerals are usually divided into two different types, 1:1 or 2:1. When one tetrahedral sheet is bonded with one octahedral sheet, then the structure is defined as a 1:1 silicate structure.[10] When an octahedral sheet is in between two tetrahedral sheets, then the structure is called 2:1 silicate structure.[10] For example, kaolinite is a 1:1 clay, montmorillonite and illite are 2:1 clays. Clay layers are held together by attractive van der Waal forces and by hydrogen bonds arising from hydroxyl groups on octahedral sheets. One unique phenomenon of clays particles is that they are often not electrically neutral. Clay particles obtain electric charge by substitution of cations in the unit layers.[9] When a tetravalent silicon ion is replaced by a trivalent aluminum ion, because of the similar morphology of the ions, a negative charge occurs.[9] This charging mechanism is known as isomorphous substitution of ions.[9] The charges on basal planes are permanent charges that are independent of pH. The primary alumina and silica bonds are broken at the edge, leading to pH dependent charges.[9]

1.3 Electrical Double Layer

The electrical double layer has an important effect on the behaviors of charged particles in colloidal systems. It affects the stability of a colloidal suspension by changing the surface charge of charged particles. The electrical double layer theory is well established. The very first model called the Helmholtz model was developed during the 1850s. It was succeeded by the Gouy-Chapman model, and more recently by the Stern model illustrated in the Figure 1.4.

The surface charge is the charge naturally carried by the particle right on the particle surface. In the Stern layer, the ions are bonded to the particle surface.[11] The slipping plane is the dividing line of the liquid and particle surface. Inside the slipping plane, it is believed that the liquid is attached to the particle surface. The electric potential at the slipping plane is called zeta potential. Zeta potential is the key indicator of the stability of a colloidal suspension, for that it is the electric potential difference between the particle surface and the suspending liquid phase. Counter ions can reduce the stability of a colloidal suspension by compressing the electrical double layer.

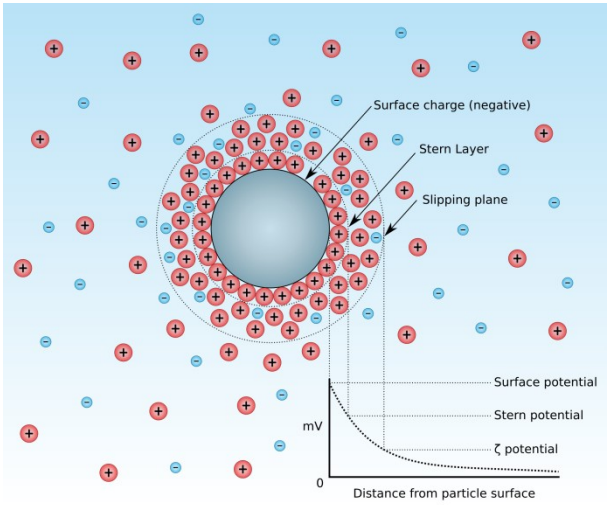

Figure 1.4 Stern model illustration for electrical double layer.[11]

1.4 DLVO Theory, Coagulation and Flocculation

The DLVO theory is named after Derjaguin, Landau, Verwey, and Overbeek.[12] It demonstrate the balance between the attractive van der Waals forces and the repulsive electrical double layer force.[12] When the repulsive electrical double layer force dominates,

then the colloidal suspension will remain stable. When the attractive van der Waals force dominates the colloidal particles aggregate, and the suspension becomes unstable. Double layer compression leads to the reduction in the repulsive force. This effect alone, realized by adding salts to the aqueous phase, can accelerate particle settlement in the tailings ponds. Additives, such as coagulants that for this application carry positive charges, can neutralize the negative charges on more than one particle surface concurrently leading to particle coagulation. Coagulants may be organic or inorganic compounds. For example, polyamine and polymelamine formaldehydes are organic coagulants. Aluminum sulfate and ferric sulfate are inorganic coagulants. Coagulated particles may continue to grow by adding individual clay particles or other coagulated particles so as form micro and then visible particle flocs. Flocculation may be aided using a cationic or anionic polymeric flocculant.[13] The larger and more densely packed the agglomeration of particles becomes the more rapidly they sediment.

1.5 Current Tailings Management and Concerns

Efforts are being made to accelerate the settlement of clays and sands in tailings, especially of mature fine tailings. The Consolidated Technology (CT) process is widely applied in the oil sands industry including by Suncor and CNRL.[14] In the CT process, gypsum is the coagulant used to accelerate the settlement of particles in suspension.[15] After the deposition process is completed, the water can be reused for oil sands extraction.[15]

Mature fine tailings drying (MFTD) is a more recent process and has some advantages over the CT process. In this process anionic polyacrylamide is added to mature fine tailings to consolidate them and to release water.[15] This is coupled with water evaporation, which also accelerates MFT deposition.[15] Figure 1.5 shows the process units and steps in the mature fine tailings drying process (MFTD) that Suncor uses.[16] In the first step, recycle water for flushing and MFT feed are processed by barge and pumps. In the screened tank, the MFT feed is screened for debris.[16] Then the polymer is added to accelerate the deposition of MFT. The MFT feed and polymer solution are mixed in the MFT polymer mixer. Finally, the MFT feed with polymer is discharged into deposition cells to deposit and dewater.

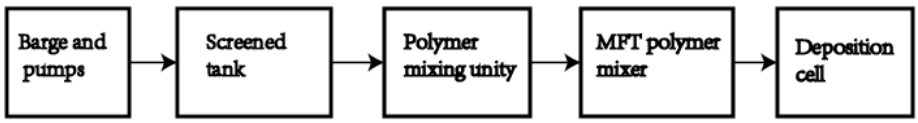

Figure 1.5 Mature fine tailings drying (MFTD) process sketch.

Even though these methods are being applied, the reclamation of tailings is still a slow process with a long-time horizon. At current mined-oil sands production rates, the current tailings ponds continue to grow in size. More effective technologies are needed to improve the current methods for managing tailings and to address the footprint of the accumulated materials in existing tailings ponds. The social license to operate facilities,

and the environmental risk linked to tailings management must be paramount within the oil sands sector.

1.6 Thesis Objectives and Outline

This research focuses on improving the fundamental understanding of the interaction of oil contaminated clay particles at oil/water interfaces in tailings ponds, in general, and on how oil properties affect clay particle adsorption at oil-water interfaces. The aim is to identify better solutions for accelerating oil water separation and clay particle settling in tailings ponds by studying the behaviors of well-defined silica core nanoparticles with well-defined organic ligands on their surface at toluene + heptane/ water interfaces. The nanoparticles under study include, bare silica nanoparticles, silylated silica nanoparticles, silylated silica−octyl nanoparticles and silylated silica−anthracene nanoparticles, with hydroxyl groups, short and long alkane chains and aromatic groups respectively on their surfaces. Both clays and functional silica nanoparticles are silica based and negatively charged. By studying functionalized silica nanoparticles, the effects of oil contaminant properties on clay behaviors can be isolated. Nanoparticle concentration, water pH and salinity comprised additional variables of interest. The results obtained are expected to provide fundamental insights and a well-defined basis for the development of settling process models.

The thesis is divided in five chapters:

Chapter 2: Literature review on fundamentals and recent research progress of interfacial tension and nanoparticles.

Chapter 3: Experimental methods, materials and mechanism are described including the illustration of four different silica nanoparticles structures.

Chapter 4: The interfacial tension measurements result. Data analysis and discussion.

Chapter 5: Main conclusions and potential future works.

1.7 References

(1) Golby, S.; Ceri, H.; Gieg, L.,M.; Chatterjee, I.; Marques, L.,L.R.; Turner, R.,J. Evaluation of Microbial Biofilm Communities from an Alberta Oil Sands Tailings Pond. *FEMS Microbiology Ecology* **2012***, 79*, 240-250.

(2) Masliyah, J.; Czarnecki, J.; Xu, Z. Handbook on Theory and Practice of Bitumen Recovery from Athabasca Oil Sands. *Theoretical Basis* **2011***, 1*.

(3) Mikula, R. J.; MuÑoz, V. A.; Omotoso, O. Centrifugation Options for Production of Dry Stackable Tailings in Surface Mined Oil Sands Tailings Management. *Journal of Canadian Petroleum Technology* **2009***, 48*, 19-23.

(4) Quagraine, E. K.; Peterson, H. G.; Headley, J. V. In Situ Bioremediation of Naphthenic Acids Contaminated Tailing Pond Waters in the Athabasca Oil Sands Region-Demonstrated Field Studies and Plausible Options: A Review. Journal of Environmental Science and Health, Part A 2005, 40, 685-722.

(5) Song, B.; Springer, J. Determination of Interfacial Tension from the Profile of a Pendant Drop using Computer-Aided Image Processing. Journal of Colloid and Interface Science 1996, 184, 64-76.

(6)Tariq Siddique; Phillip M Fedorak; Michael D MacKinnon; Julia M Foght Metabolism of BTEX and Naphtha Compounds to Methane in Oil Sands Tailings. Environmental science & technology 2007, 41, 2350-2356.

(7) OIL SANDS MAGAZINE TAILINGS PONDS 101.

http://www.oilsandsmagazine.com/technical/mining/tailings-ponds.

(8) Song, B.; Springer, J. Determination of Interfacial Tension from the Profile of a Pendant Drop using Computer-Aided Image Processing. *Journal of Colloid and Interface Science* **1996**, *184*, 64-76.

(9) Hunter, R. J. In *Foundations of Colloid Science;* Oxford University Press: New York, 2001; 25-28.

(10) Madejová, J. FTIR Techniques in Clay Mineral Studies. *Vibrational Spectroscopy* **2003**, *31*, 1-10.

(11) Henderson, D. Recent Progress in the Theory of the Electric Double Layer. *Prog Surf Sci* **1983**, *13*, 197-224.

(12) Hermansson, M. The DLVO Theory in Microbial Adhesion. *Colloids and Surfaces B: Biointerfaces* **1999**, *14*, 105-119.

(13) Gregory, J.; O'Melia, C. R. Fundamentals of Flocculation. *Crit. Rev. Environ. Sci. Technol.* **1989**, *19*, 185-230.

(14) Chan, M. C. W. A Novel Flocculant for Enhanced Dewatering of Oil Sands Tailings, ProQuest Dissertations Publishing, 2011.

(15) World Wildlife Fund In *Tailings, a lasting oil sands legacy;* World Wildlife Fund Canada: Toronto, Ont., 2010; 40.

(16) Suncor Energy Inc. SUNCOR ENERGY INC. Oil Sands DDA Plan Prepared in accordance with Directive 074 – Appendix C, 2010.

CHAPTER 2: LITERATURE REVIEW

2.1 Fundamentals of Interfacial Tension

Interfacial tension is closely related to daily life - from lattes, to sauces, to smoothies. Foams and emulsions form due to interfacial tension, and their stability is determined by the interfacial tension value. Interfacial tension can also describe the surface activity of surfactants, fine particles and other surface-active materials quantitatively. It plays key roles in many industrial processes.

2.1.1 Definition of Interfacial Tension

Figure 2.1 shows the interfacial tension between two immiscible liquids. The dots in white and blue stand for molecules in the phases 1 and 2 respectively. The arrows stand for the cohesive forces between the liquid molecules in different directions. Interfacial tension exists between two immiscible fluids. It is the Gibbs free energy per unit area at constant temperature, pressure, and global composition.[1] It is defined as:

$$dG=\gamma dA \qquad (2.1)$$

Where γ is the interfacial tension and dA is the change in area.

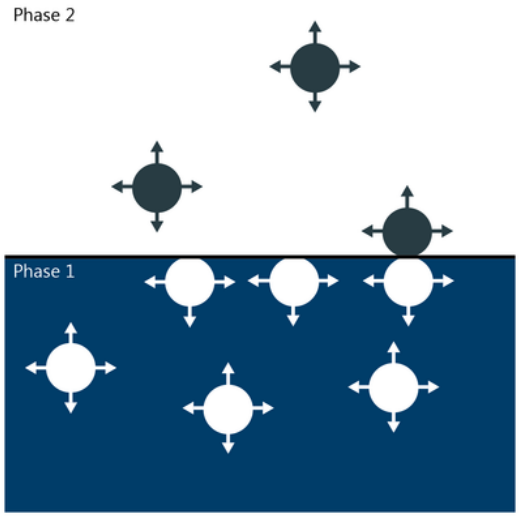

Figure 2.1 Schematic diagram of interfacial tension between two immiscible phases.[2]

2.2 Adsorption Isotherms

Adsorption is the adhesion of gas, liquid, particles or dissolved solid on to an interface by diffusion.[3] Adsorption is usually studied through adsorption isotherms,[3] and can be governed by physical or chemical interactions with species at the interface. Physical adsorption is dominated by van der Waals interactions and is reversible. Adsorption and desorption processes are concurrent and a steady state is reached over time at fixed temperature and pressure. Typically chemical adsorption is irreversible at fixed temperature and pressure. For adsorption at liquid-liquid interfaces, the Gibbs, Langmuir and Szyszkowski isotherms[4] are commonly used to describe the interaction between the amount of adsorbate on an interface and its concentration in the bulk at a constant temperature and pressure.[5]

2.2.1 Gibbs Adsorption Isotherm

The surface excess concentration (Γ_i) of adsorbate '*i*' is the amount of adsorbate adsorbed on an interface per unit area. It can be obtained from interfacial tension measurements through equation 2.2:

$$d\gamma = -\sum_i \Gamma_i d\mu_i \tag{2.2}$$

where γ is the interfacial tension, Γ_i is the surface excess concentration and μ_i is the chemical potential. The chemical potential can be expressed as:

$$d\mu_i = RTd\ln a_i \tag{2.3}$$

where a_i is the activity of adsorbate '*i*' in the bulk phase, *R* is ideal gas constant, *T* is the temperature. Thus,

$$d\gamma = -RT\sum_i \Gamma_i d\ln a_i \tag{2.4}$$

If the solution of '*i*' is diluted, the activity coefficient is well approximated as the infinite dilution activity coefficient, which is independent of composition. Equation 2.4 can be written as:

$$d\gamma = -RT\sum_i \Gamma_i d\ln C \tag{2.5}$$

where *C* is the molar concentration of component '*i*'.

At constant temperature, equation 2.5 becomes:

$$\Gamma = -\frac{1}{RT}\left(\frac{d\gamma}{d\ln C}\right) \tag{2.6}$$

Thus the surface excess concentration Γ can be obtained from a plot interfacial tension γ versus log C and with further calculation, the area occupied by each molecule can also be calculated as:

$$\mathrm{a} = \frac{1}{N_A \Gamma} \tag{2.7}$$

And this in turn can help us understand the orientation and the arrangement of adsorbate molecules on the interface.

2.2.2 Langmuir Adsorption Isotherm

In 1916 Langmuir introduced surface coverage 'θ' into the system. He supposed that for a certain system, the number of adsorption sites is a constant. The surface coverage 'θ' is the percentage of the adsorption sites occupied. It can be defined as

$$\theta = \frac{\Gamma_i}{\Gamma_{\max}} = \frac{K_L}{1 + K_L C} \tag{2.8}$$

where Γ_{max} is the maximum surface excess concentration, K_L is the equilibrium adsorption constant, C is the bulk concentration of adsorbate. Equation 2.8 was first designed to describe gas adsorption where pressure has a big impact. The Langmuir adsorption isotherm can only be used for monolayers on an interface. By combining equations 2.5 and 2.7:

$$d\gamma = -RT\Gamma_{max} \ln\left(1 + K_L C\right) \tag{2.9}$$

2.3 Effect of pH on Interfacial Tension

For oil-water systems, the interfacial tension usually decreases with increasing temperature. The pH can also affect the interfacial tension between oil and water in a significant way.[6] Crude oil contains natural surfactant components like asphaltenes and naphthenic acids. In tailings ponds, where sand and clays are always contaminated by crude oil, they can also adsorb on the oil/water interface to form Pickering emulsions which are emulsions stabilized by solid particles. Changes in the pH in the aqueous phase can affect the acidic components in the crude oil such as naphthenic acids.[7] The dissociation of acidic components is impacted in both acidic and alkaline environments, but alkaline environments have a stronger impact on disassociation. In addition, hydroxide ions can adsorb on liquid-liquid interfaces, which in addition can decrease the interfacial tension (IFT).[8] Surface active anions are released due to dissociation of acidic components especially in alkaline environments. Stressner found that for oil-in-brine emulsions the best pH range for emulsion breakage is 6 to 8.[6] This indicates that the interfacial tension between oil and water reaches highest value in this range. Acevedo et al., found that for heavy crude oil/water mixtures, the interfacial tension versus pH plots are bell-shaped.[9] Poteau et al.,[10] found that asphaltenes that serve as surfactants at oil/water interfaces, become charged when the pH is high or low.[10] Figure 2.2 shows how the interfacial tension between oil and water change with pH. The effect of pH on interfacial tension is almost uniform for different oil + water mixtures. The highest

interfacial tension is achieved at ~ pH 7. Alkaline environments have the most significant impact on interfacial tension.

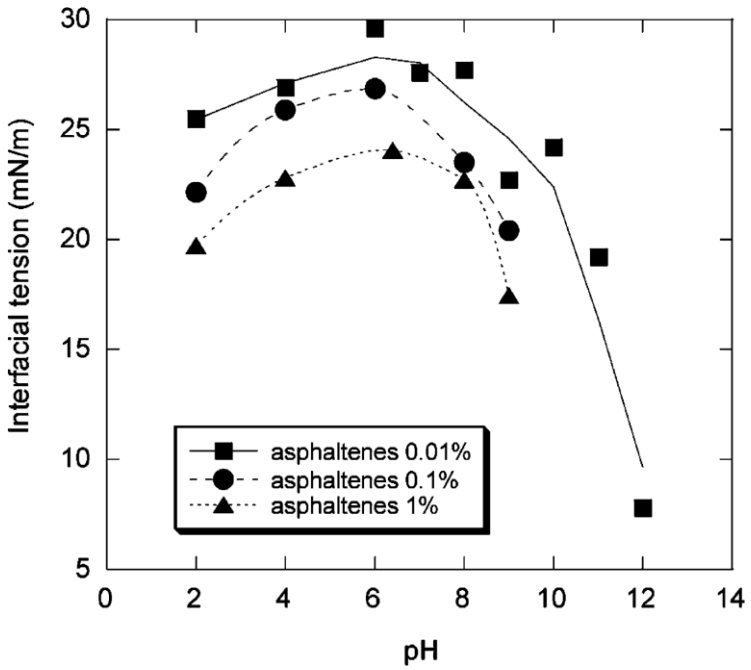

Figure 2.2 Venezuelan heavy crude oil-water interfacial tension vs. pH at 298 K and 5400 s.[10] Asphaltene concentration is a parameter.

2.4 Effect of Salinity on Interfacial Tension

If there is no surfactant present, the interfacial tension between oil and water usually increases with the salinity of the aqueous phase. For oil/water systems with surfactants, the adsorption of surfactant at an interface can be affected by added salt.[11] Both kinetic and equilibrium effects are observed. For example, Mackay et al., found that with salt in the aqueous phase, interfacial tensions decreased.[12] In 1996, Cai et al., found that with higher salinity, interfacial tension increased.[13] Lashkarbolooki *et al*., found that the

interfacial tensions between crude oil and brines can both increase and decrease with different salts and concentrations,[14] as shown in Figure 2.3. The well-known "Salting-in''[15] effect increases the critical micelle concentration of surfactants by increasing the ionic strength which can increase the solubility of solute.[13] The "Salting out" effect hinders diffusion of surfactant to the interface[11, 15] and induces micelle formation in the aqueous phase.[16] Salts can also promote diffusion of surfactants,[17] thus, accelerating adsorption. The impact of salt concentration on the interfacial tension of specific oil water surfactant systems is complex and still merits individualized study.

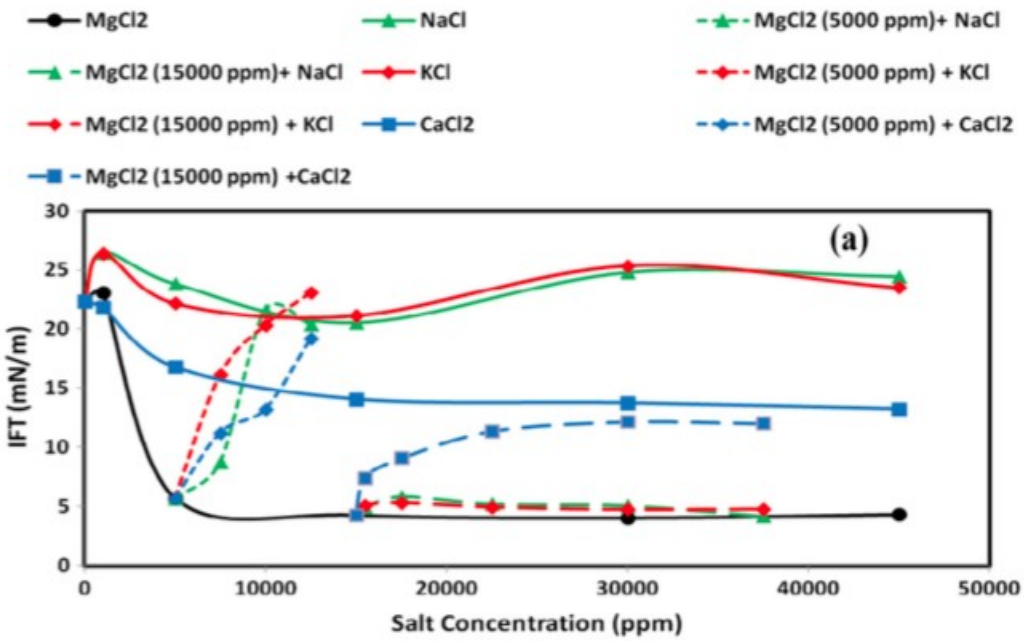

Figure 2.3 Interfacial tension between crude oil and brine. Salt concentration is a parameter.[14]

2.5 Effect of Temperature and Pressure on Oil/Water Interfacial Tension

Typically interfacial tension decreases with increasing temperature and pressure. Diffusion of surfactants is accelerated at higher temperatures. At higher temperatures and pressures, the solubility of oil in water and water in oil increase which leads to a decrease in interfacial tension. For example, the interfacial tension between benzene/decane and water decreases from 34 mN/m at 25 °C to 15 mN/m at 176 °C.[18] The interfacial tension between poly lactic acid and carbon dioxide decreases with increasing temperature and pressure[19] as shown in Figure 2.4. However, counter examples can also be found. For example, the interfacial tension between methane + n-decane and water increases with increasing temperature in the range from 23 °C to 100 °C.[20] At 50 °C, the interfacial tension between water and n-alkanes increases with pressure.[13] The curves are shown in Figure 2.5.

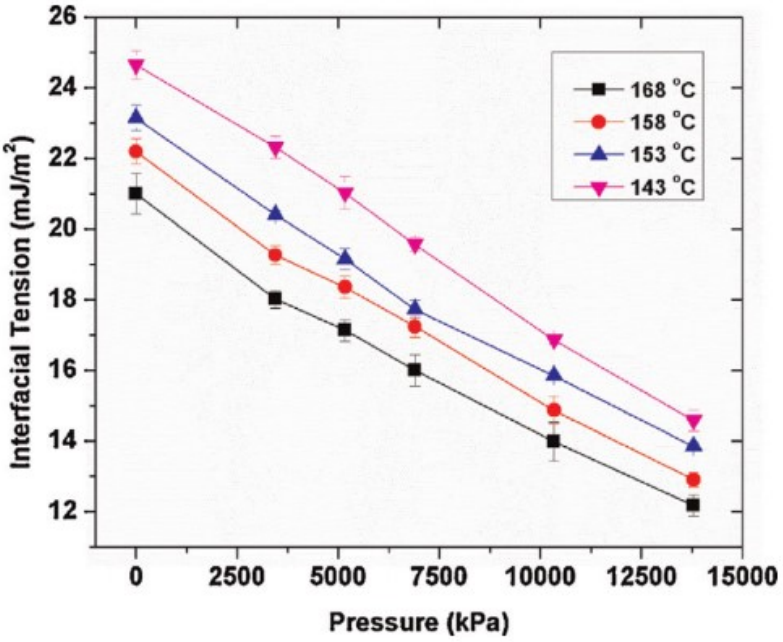

Figure 2.4 Interfacial tension between poly lactic acid and carbon dioxide as a function of pressure. Temperature is a parameter.[19]

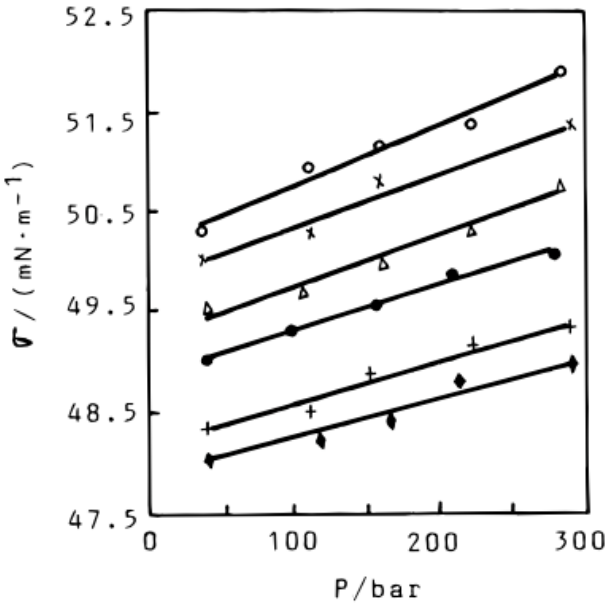

Figure 2.5 Pressure effect on interfacial tension for *n*-alkane + water mixtures at 50.0 °C: (○) C_{16}; (×) C_{14}; (△) C_{12}; (●) C_{10}; (+) C_8; (♦) C_6.[13]

2.6 Crude Oil Chemistry

Crude oils are naturally occurring resources consisting of hundreds of thousands of hydrocarbon and substituted hydrocarbon components that vary with origin.[21] Whether they are characterized as light crude oils, medium crude oils, heavy crude oils or bitumen by their relative density[22] and transport properties such as viscosity, all crude oils include compounds with a broad spectrum of molar masses, molecular structures, and elemental compositions. Constituents such as naphthenic and sulfonic acids are surface active. They reduce the interfacial tension between oil and water and stabilize the emulsions. Shaw et al., showed with a series of publications that pentane asphaltene rich nanoparticles could be separated from Athabasca bitumen, Maya crude oil and Safaniya vacuum residue without adding solvents.[23, 24, 25] Related but chemically separated asphaltene fractions aggregate in toluene,[26] have high affinity to some surfaces such as alumina and silica oxides,[27] and are active at oil water interfaces.[28, 29] Asphaltenes can form rigid films on water drops, which prevent them from coalescing. For mined bitumen, these species are present in mine tailings, in addition to clays.

2.7 Nanoparticles Research Progress and Applications

Nanotechnology is an exploding field with papers published and patents granted by the thousands annually.[30] Nanoparticle related research is an active part of this field. Nanoparticles with diameters ranging from 1-100 nm have very large surface area to volume ratios, and are being designed for applications as diverse as drug delivery, cosmetics, processed food, materials synthesis, optics, and oil production, and they can be found in natural or disturbed environments, hydrocarbon resources, to cite but a few

examples. The interactions between nanoparticles in nanofluids (nanoparticles in suspension[31]) and their interactions with interfaces, the focus of this work, include Brownian motion, van der Waals interactions, hydrogen bonding,[31] steric hinderance,[32] magnetic interaction,[33] etc.

The structures of nanoparticles are diverse. Figure 2.6 shows six different structures. Gold nanoparticles with a core-shell structure are used as catalysts.[34] Bifunctional nanoparticles were synthesized by Niemeyer et al.,[35] Malikova et al., assembled gold nanoparticles layer-by-layer.[36] They discovered a surface plasmon absorption band which indicates the strong interaction between adjacent layers.[36] The yolk-shell structure is first introduced by Yin et al., in 2004.[37] The structure of yolk-shell is different from core-shell, because the core of york-shell structure can move freely inside the shell, while the core of core-shell structures is attached to the shell. Hollow nanoparticles, are used for drug delivery.

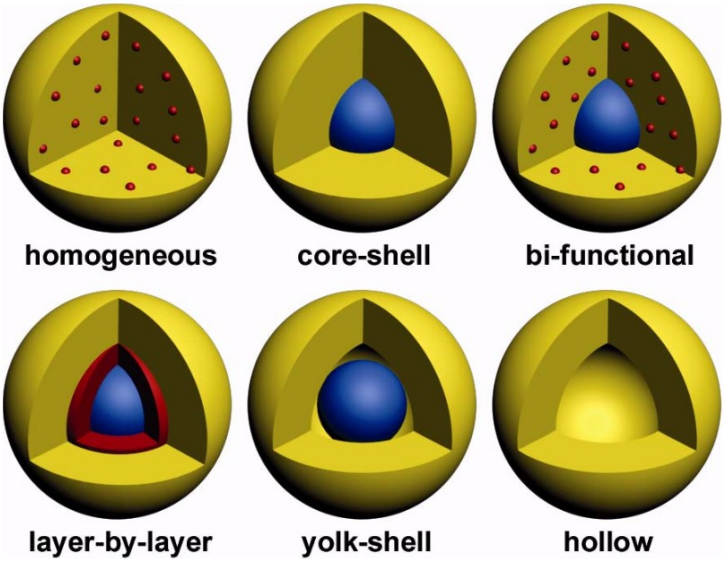

Figure 2.6 Different structures of nanoparticles.[38]

2.7.1 Silica Nanoparticles Properties and Applications

As nanotechnology develops, different nanodevices have found application in electronic, magnetic, mechanical, and biological studies such as carbon nanotubes, nano-magnetics, quantum dots, and polymer micelles.[39] Silica nanoparticles are widely used in chemical and biomedical research. They are non-toxic and biocompatible, and can be functionalized for fundamental studies. They have high thermal stability and electro inactivity in the aqueous phase. Silica nanoparticles do carry negative charges on their surface that make them great mimics for clays that are similarly charged.

2.7.2 Functionalized Silica Nanoparticles

Functionalized nanoparticles are widely used as carriers, markers, probes and so on. Silica nanoparticles are an excellent base for functionalization by reaction with silanol groups on the particle surface. Amino, mercapto, carboxyl groups and aliphatic chains can be added.[38] They can also be functionalized with DNA, proteins, antibodies and other biochemical molecules.[38]

Different methods are applied to functionalize bare silica nanoparticles. An et al., demonstrated a simple method to synthesize carboxylic acid-functionalized silica nanoparticles.[40] The process of synthesis is shown in Figure 2.7. First amino-functionalized silica nanoparticles (SiO_2–NH_2) are prepared. Then the amino-functionalized silica dispersion is used to functionalize nanoparticles with carboxyl groups.[40]

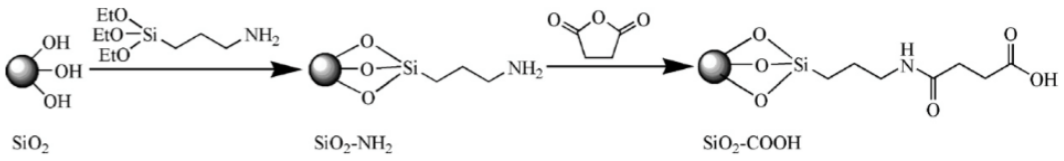

Figure 2.7 Mechanism of carboxylic acid-functionalized silica Nanoparticles Synthesis.[40]

Aubert et al., synthesized silica nanoparticles using a water-in-oil microemulsion.[41] Surfactants are really important in this approach because surfactant choice impacts the size and shape of the functionalized silica nanoparticles.[42, 43] The method is highly reproducible for different nanoparticles. The size and shape of nanoparticles in Aubert's study are well controlled which makes the method promising for biochemical and catalyst preparation applications.

2.7.3 Silica Nanoparticles as Emulsion Stabilizers

Surfactants, fine solid particles, large molecules like proteins, are typical emulsion stabilizers. All of them can adsorb on the interface between two liquid phases and lower the interfacial tension. When the emulsions are stabilized by solid particles, they are called Pickering emulsions. Particles adsorbed on an interface can prevent drops from coalescing. The difference between surfactant stabilized emulsions and solid particle stabilized emulsions is shown in Figure 2.8.

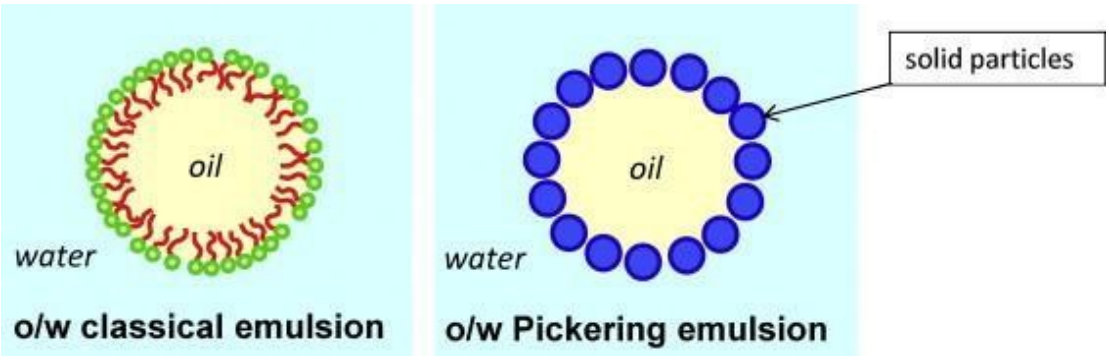

Figure 2.8 Oil-in-Water classical emulsion and oil-in-water Pickering emulsion.[44]

There are similarities as well as differences between surfactants and fine solid particles. Both of them can adsorb on the liquid-liquid interface,[45] but particle adsorption is irreversible because the free energy of detachment is usually much higher than thermal energy (kT).[46] Also, the molecular mass of surfactants is lower than that of solid nanoparticles. Surfactants are amphiphilic while nanoparticles may have homogeneous, Janus, or multipli active surfaces.

For homogeneous solid particles, the contact angle of solid particles at an interface determines their surface activity. If all of the particles are the same size and are spherical, the free energy of particle detachment is directly related to the contact angle measured in the aqueous phase, which increases with contact angle from 0° to 90° (maximum) and decreases after 90°.[47] Figure 2.9 shows how particles with different contact angles behave on an interface. In addition, larger particles require more energy for detachment. The free energy of detachment for a single particle can be expressed as:

$$E = \pi r^2 \gamma \left(1 \pm \cos\theta\right)^2 \tag{2.10}$$

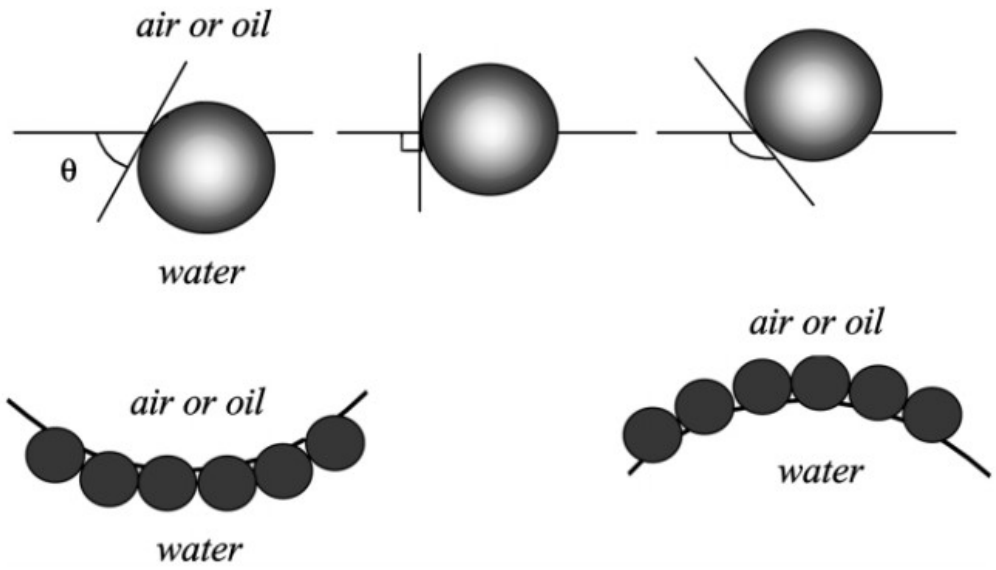

Figure 2.9 Particles adsorbed on water/oil or water/air interfaces with different contact angles.[37]

Hydrophobic silica particles can stabilize oil-in-water emulsions. Hydrophilic silica particles can stabilize water-in-oil emulsions.[47] Interfaces need not be fully covered by a coherent particle layer to be stabilized.[46] If the particle layers are full and coherent, then the emulsions remain stable for years because of steric hindrance. For partially covered interfaces, emulsions are stabilized by bridging monolayers of particles between drops.[46] However, the mechanism for silica particle stabilized emulsions is not fully understood and studies continue to be performed with ambiguous outcomes[45] and more systematic research is warranted.

2.8 Summary

Clays and sand particles commonly stabilize oil in water and water in oil emulsions found in the oil sands industry through their impact on interfacial tension. The interfacial tension between two immiscible liquids can be influenced by many factors including pH, salinity, temperature, pressure and surfactant concentration. Functionalized silica nanoparticles are used in this work to mimic behaviors of oil contaminated clay and sand particles in tailings ponds. By functionalizing the silica nanoparticles with a variety of functional groups, the effect of different oil contaminant classes can be isolated and evaluated in relation to impacts related to other well-known variables surveyed with these particles, the influence of silica nanoparticle surface composition and particle concentration on dynamic and steady state interfacial tension values is investigated as a function of water pH and salinity, and oil phase composition.

2.9 References

(1) Gibbs, J. W. In *The Scientific Papers of J. Willard Gibbs;* Dover: New York, 1961; Vol. 1, pp 55-371.

(2) KRUSS Interfacial tension. *https://www.kruss.de/services/education-theory/glossary/interfacial-tension/*.

(3) J. G. Calvert Glossary of Atmospheric Chemistry Terms (Recommendations 1990). *Pure and Applied Chemistry* **1990***, 62*, 2167-2219.

(4) Rosen, M. J.; Kunjappu, J. T. In *Surfactants and Interfacial Phenomena;* John Wiley & Sons: Hoboken, 2012; pp 618.

(5) Foo, K. Y.; Hameed, B. H. Insights into the Modeling of Adsorption Isotherm Systems. Chemical Engineering Journal 2010, 156, 2-10.

(6) STRASSNER, J. E. Effect of pH on Interfacial Films and Stability of Crude Oil-Water Emulsions. *Journal of Petroleum Technology* **1968***, 20*, 303-312.

(7) Havre, T. E.; Sjöblom, J.; Vindstad, J. E. Oil/Water-partitioning and Interfacial Behavior of Naphthenic Acids. *J. Dispersion Sci. Technol.* **2003***, 24*, 789-801.

(8) Speight, J. G. In *Lange's handbook of chemistry;* McGraw-Hill New York: 2005; Vol. 1.

(9) Acevedo, S.; Escobar, G.; Gutiérrez, L.; Rivas, H. Isolation and Characterization of Natural Surfactants from Extra Heavy Crude Oils, Asphaltenes and Maltenes. Interpretation of their Interfacial Tension-pH Behaviour in Terms of Ion Pair Formation. *Fuel* **1992***, 71*, 619-623.

(10) Poteau, S.; Argillier, J.; Langevin, D.; Pincet, F.; Perez, E. Influence of pH on Stability and Dynamic Properties of Asphaltenes and Other Amphiphilic Molecules at the Oil−Water Interface. Energy & Fuels 2005, 19, 1337-1341.

(11) Denoyel, R.; Rouquerol, J. Thermodynamic (Including Microcalorimetry) Study of the Adsorption of Nonionic and Anionic Surfactants Onto Silica, Kaolin, and Alumina. *J. Colloid Interface Sci.* **1991***, 143*, 555-572.

(12) Mackay, D.; Hossain, K. Interfacial Tensions of Oil, Water, Chemical Dispersant Systems. *The Canadian Journal of Chemical Engineering* **1982***, 60*, 546-550.

(13) Cai, B.; Yang, J.; Guo, T. Interfacial Tension of Hydrocarbon Water/Brine Systems Under High Pressure. *Journal of chemical & engineering data* **1996***, 41*, 493-496.

(14) Lashkarbolooki, M.; Riazi, M.; Ayatollahi, S.; Hezave, A. Z. Synergy Effects of Ions, Resin, and Asphaltene on Interfacial Tension of Acidic Crude Oil and Low–high Salinity Brines. *Fuel* **2016***, 165*, 75-85.

(15) Schott, H.; Royce, A. E.; Han, S. K. Effect of Inorganic Additives on Solutions of Nonionic Surfactants: VII. Cloud Point Shift Values of Individual Ions. *J. Colloid Interface Sci.* **1984***, 98*, 196-201.

(16) Somasundaran, P. In *Encyclopedia of surface and colloid science;* CRC Press: Boca Raton, Fla. [u.a.], 2016; 54-68.

(17) Bai, J.; Fan, W.; Nan, G.; Li, S.; Yu, B. Influence of Interaction between Heavy Oil Components and Petroleum Sulfonate on the Oil–water Interfacial Tension. *J. Dispersion Sci. Technol.* **2010***, 31*, 551-556.

(18) Jennings, H. Y. The Effect of Temperature and Pressure on the Interfacial Tension of Benzene-Water and Normal Decane-Water. *Journal of Colloid and Interface Science* **1967***, 24*, 323-329.

(19) Sarikhani, K.; Jeddi, K.; Thompson, R. B.; Park, C. B.; Chen, P. Effect of Pressure and Temperature on Interfacial Tension of Poly Lactic Acid Melt in Supercritical Carbon Dioxide. *Thermochimica Acta* **2015***, 609*, 1-6.

(20) Jennings Jr, H. Y.; Newman, G. H. The Effect of Temperature and Pressure on the Interfacial Tension of Water Against Methane-Normal Decane Mixtures. *Society of Petroleum Engineers Journal* **1971***, 11*, 171-175.

(21) Hughey, C. A.; Rodgers, R. P.; Marshall, A. G. Resolution of 11 000 Compositionally Distinct Components in a Single Electrospray Ionization Fourier Transform Ion Cyclotron Resonance Mass Spectrum of Crude Oil. *Anal. Chem.* **2002***, 74*, 4145-4149.

(22) Simanzhenkov, V.; Idem, R. In *Crude oil chemistry;* Marcel Dekker: New York, 2003; pp 409.

(23) Bazyleva, A., Becerra, M., Stratiychuk-Dear, D., and Shaw, J. M., Phase behavior of Safaniya vacuum residue. Fluid Phase Equilibria, 2014. 380(0): p. 28-38.

(24) Zhao, B.; Shaw, J. M. Composition and Size Distribution of Coherent Nanostructures in Athabasca Bitumen and Maya Crude Oil. *Energy & Fuels* **2007***, 21*, 2795-2804.

(25) Eyssautier, J. l., Espinat, D., Gummel, J. r. m., Levitz, P., Becerra, M., Shaw, J., and Barré, L., Mesoscale Organization in a Physically Separated Vacuum Residue: Comparison to Asphaltenes in a Simple Solvent. Energy & Fuels, 2012. 26(5): p. 2680-2687.

(26) Spiecker, P. M.; Gawrys, K. L.; Trail, C. B.; Kilpatrick, P. K. Effects of Petroleum Resins on Asphaltene Aggregation and Water-in-Oil Emulsion Formation. *Colloids Surf. Physicochem. Eng. Aspects* **2003***, 220*, 9-27.

(27) Gray, M. R. In *Upgrading Oilsands Bitumen and Heavy Oil;* Pica Pica Press: Edmonton, 2015; 2-6.

(28) Tsamantakis, C.; Masliyah, J.; Yeung, A.; Gentzis, T. Investigation of the Interfacial Properties of Water-in-Diluted-Bitumen Emulsions using Micropipette Techniques. *J. Colloid Interface Sci.* **2005***, 284*, 176-183.

(29) Yarranton, H. W.; Hussein, H.; Masliyah, J. H. Water-in-Hydrocarbon Emulsions Stabilized by Asphaltenes at Low Concentrations. *J. Colloid Interface Sci.* **2000***, 228*, 52-63.

(30) Huang, C.; Notten, A.; Rasters, N. Nanoscience and Technology Publications and Patents: A Review of Social Science Studies and Search Strategies. *The Journal of Technology Transfer* **2011***, 36*, 145-172.

(31) Taylor, R.; Coulombe, S.; Otanicar, T.; Phelan, P.; Gunawan, A.; Lv, W.; Rosengarten, G.; Prasher, R.; Tyagi, H. Small Particles, Big Impacts: A Review of the Diverse Applications of Nanofluids. *J. Appl. Phys.* **2013***, 113*, 1.

(32) Schiffelers, R. M.; Ansari, A.; Xu, J.; Zhou, Q.; Tang, Q.; Storm, G.; Molema, G.; Lu, P. Y.; Scaria, P. V.; Woodle, M. C. Cancer siRNA Therapy by Tumor Selective Delivery with Ligand-Targeted Sterically Stabilized Nanoparticle. *Nucleic Acids Res.* **2004***, 32*, e149.

(33) Mrup, S.; Hansen, M. F.; Frandsen, C. Magnetic Interactions between Nanoparticles. *Beilstein journal of nanotechnology* **2010***, 1*, 182.

(34) Zhong, C.; Maye, M. M. Core–shell Assembled Nanoparticles as Catalysts. *Adv Mater* **2001***, 13*, 1507-1511.

(35) Niemeyer, C. M.; Ceyhan, B.; Noyong, M.; Simon, U. Bifunctional DNA–gold Nanoparticle Conjugates as Building Blocks for the Self-Assembly of Cross-Linked Particle Layers. *Biochem. Biophys. Res. Commun.* **2003***, 311*, 995-999.

(36) Malikova, N.; Pastoriza-Santos, I.; Schierhorn, M.; Kotov, N. A.; Liz-Marzn, L. M. Layer-by-Layer Assembled Mixed Spherical and Planar Gold Nanoparticles: Control of Interparticle Interactions. *Langmuir* **2002***, 18*, 3694-3697.

(37) Yin, Y.; Rioux, R. M.; Erdonmez, C. K.; Hughes, S.; Somorjai, G. A.; Alivisatos, A. P. Formation of Hollow Nanocrystals through the Nanoscale Kirkendall Effect. *Science* **2004***, 304*, 711-714.

(38) Vivero-Escoto, J. In *Silica nanoparticles;* Chemical engineering methods and technology; Nova Science Publishers: New York, 2012; , pp 288.

(39) Bharti, C.; Nagaich, U.; Pal, A. K.; Gulati, N. Mesoporous Silica Nanoparticles in Target Drug Delivery System: A Review. *International journal of pharmaceutical investigation* **2015***, 5*, 124.

(40) An, Y.; Chen, M.; Xue, Q.; Liu, W. Preparation and Self-Assembly of Carboxylic Acid-Functionalized Silica. *J. Colloid Interface Sci.* **2007***, 311*, 507-513.

(41) Aubert, T.; Grasset, F.; Mornet, S.; Duguet, E.; Cador, O.; Cordier, S.; Molard, Y.; Demange, V.; Mortier, M.; Haneda, H. Functional Silica Nanoparticles Synthesized by Water-in-Oil Microemulsion Processes. *J. Colloid Interface Sci.* **2010***, 341*, 201-208.

(42) Kumar, P.; Mittal, K. L. In *Handbook of microemulsion science and technology;* CRC press: 1999; 45-47.

(43) López-Quintela, M. A.; Tojo, C.; Blanco, M. C.; Rio, L. G.; Leis, J. R. Microemulsion Dynamics and Reactions in Microemulsions. *Current opinion in colloid & interface science* **2004***, 9*, 264-278.

(44) Chevalier, Y.; Bolzinger, M. Emulsions Stabilized with Solid Nanoparticles: Pickering Emulsions. *Colloids Surf. Physicochem. Eng. Aspects* **2013***, 439*, 23-34.

(45) Binks, B. P. Particles as Surfactants—similarities and Differences. *Current opinion in colloid & interface science* **2002***, 7*, 21-41.

(46) Horozov, T. S.; Binks, B. P. Particle-Stabilized Emulsions: A Bilayer Or a Bridging Monolayer? *Angewandte Chemie International Edition* **2006***, 45*, 773-776.

(47) Binks, B. P.; Horozov, T. S. In *Colloidal particles at liquid interfaces;* Cambridge University Press: 2006;1-6 .

CHAPTER 3: EXPERIMENTAL

In this chapter the materials, samples, experimental methods and equipment supporting pendant-drop dynamic interfacial tension measurements, for functionalized silica nanoparticles dispersed in toluene or (volume ratio 50:50) mixtures of toluene + heptane at aqueous interfaces are described.

3.1 Materials

All the materials involved in this work are listed in **Table 3.1** including the information of their purity and suppliers.

Table 3.1 Materials Information.

Compound	Purity	Supplier
toluene	99.9%	Fisher Scientific
n-heptane	99%	Fisher Scientific
Hexamethyldisiloxane (HMDSO)	≥ 99.5 %	Sigma Aldrich
9-(Chloromethyl)anthracene	≥ 98%.	Sigma Aldrich
silicon oxide colloidal dispersion 15% in water	NA	Alfa Aesar
sodium bicarbonate	≥ 99.7%	Sigma Aldrich
anhydrous acetonitrile	99.8%	Sigma Aldrich
acetic acid	≥ 99%	Sigma Aldrich
(3-Mercaptopropyl) triethoxysilane	94%	Alfa Aesar
trimethylchlorosilane (TMCS)	≥ 99%	Sigma Aldrich
sodium hydroxide	≥ 99.99%	Fisher Scientific
hydrochloric acid	37.2%.	Fisher Scientific
Calcium chloride	96.5%	Fisher Scientific
sodium chloride	≥99.9%	Fisher Scientific

3.2 Silylated Silica-Anthracene Nanoparticle Synthesis

The synthesis of silica-anthracene nanoparticles largely followed the procedure of Calero et al., [1] which has three main steps. The first step is to synthesize the reagent, 3-[(Anthracen-10-yl) methylthio] propyltriethoxysilane that functions as the ligand. The

second step is to attach the ligand onto the silica nanoparticle surface. The third step is to replace hydroxyl groups on nanoparticle surfaces with trimethylsilane ligands.

Step 1: To synthesize 3-[(Anthracen-10-yl)methylthio]propyltriethoxysilane , 4.00 g (16.8 mmol) of 9-(Chloromethyl)anthracene and 4.24 g (16.8 mmol) of (3-mercaptopropyl)triethoxysilane were added in 100 mL of anhydrous acetonitrile and stirred until dissolved. Then, 7.20 g of potassium carbonate (3.6 g, 26 mmol) was put into the mixture and heated to 80 °C under reflux for 24 h. After heating, the mixture was filtered to remove solid potassium carbonate. The liquid mixture was evaporated to remove acetonitrile. The mixture was filtered to remove solid potassium carbonate. The acetonitrile was evaporated after filtration. 2.8 g of 3-[(Anthracen-10-yl)methylthio]propyltriethoxysilane was synthesized as a yellow and viscous oil.

Step 2: In a clean 2 L tri-necked flask, 800 mL of ethanol, 400 mL of water and 400 mL acetic acid were added. 1.6g of 3-[(Anthracen-10-yl)methylthio] propyltriethoxysilane was added to the mixture and stirred until the powder was dissolved. The suspension of silica nanoparticles was injected by syringe to the center of the flask while the mixture was stirred vigorously. The reagent was very hard to dissolve. Thus the mixture was heated to 80 °C and stirred for 48 hours. The ethanol was removed under rotary evaporation. Solid sodium bicarbonate ($NaHCO_3$) was then added to the mixture to adjust the pH (Fisher Accumet XL 200 pH/ Conductivity Benchtop Meter) until the pH was between 5 and 6. The silica nanoparticles were then centrifuged and washed with water and acetone twice,[2] and dried at 70 °C in vacuum oven.

Step 3: Silica nanoparticles were dispersed in anhydrous toluene in a 3L three-necked flask. The flask was set in an oil bath at 40 °C. Trimethylchlorosilane (TMCS) and hexamethyldisiloxane (HMDSO) were injected into the flask. The reaction is slow and took 24 h to finish. The solvent was removed using a rotary evaporator (BUCHI Rotavapor Model R-210). Silica nanoparticles were washed with acetone and separated by centrifugation.[3] Then, the solid separated was dried and crushed into powder.

3.3 Functionalized Silica Nanoparticles Structures and Properties

Four types of silica nanoparticles, prepared and characterized by Dr. Yeganeh Khaniani[4] were used in experiments. They included silica nanoparticles with no functional groups, silylated silica nanoparticles, silylated octyl-functionalized silica nanoparticles and alkyl-anthracene functionalized silica nanoparticles. The bare silica nanoparticles with a diameter of 4 nm are naturally hydrophilic. The surface of silica nanoparticles contain both silanol and siloxane groups. From thermogravimetric analysis (TGA), the -OH groups are about 3.1 mmol/g. There are 100 to 140 -OH groups on individual silica nanoparticle surfaces. The surface structure of silica nanoparticles is shown in Figure 3.1.

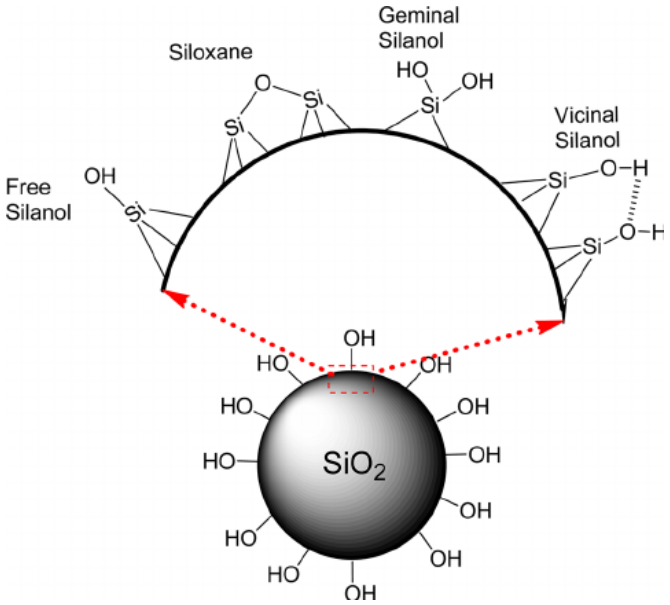

Figure 3.1 Classification of silanol groups on silica nanoparticles surface.[5]

Silylated silica nanoparticles have trimethylsilane (-Si(CH_3)$_3$) groups in addition to hydroxyl groups and residual silanol groups on their surface. From TGA analysis, the amount of functional groups is around 1.1mmol/g. Silylated silica nanoparticles have about 60 functional groups (-Si(CH_3)$_3$) and 40 to 80 hydroxyl groups (-OH) on each particle surface. The structure of silylated silica nanoparticles is shown in Figure 3.2.

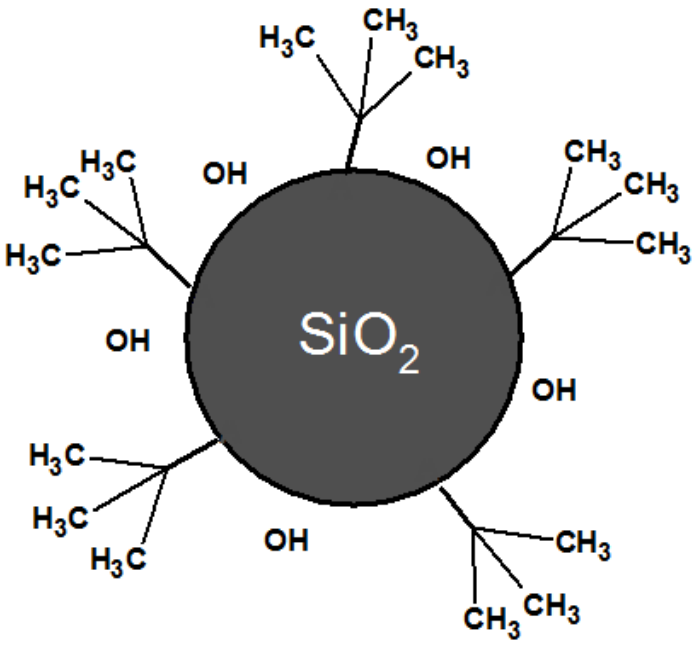

Figure 3.2 Silylated silica nanoparticle structure.

Silylated silica-octyl nanoparticles are functionalized with octyl and trimethylsilane groups. From TGA analysis, the octyl groups are 2.4 mmol/g. Trimethylsilane groups are about 0.4 mmol/g. On each silylated silica-octyl nanoparticle, there are about 100 octyl (-C_8H_{17}) chains, 11 trimethylsilane groups and residual silanol groups are less than 30. The structure of silylated silica-octyl is shown in Figure 3.3.

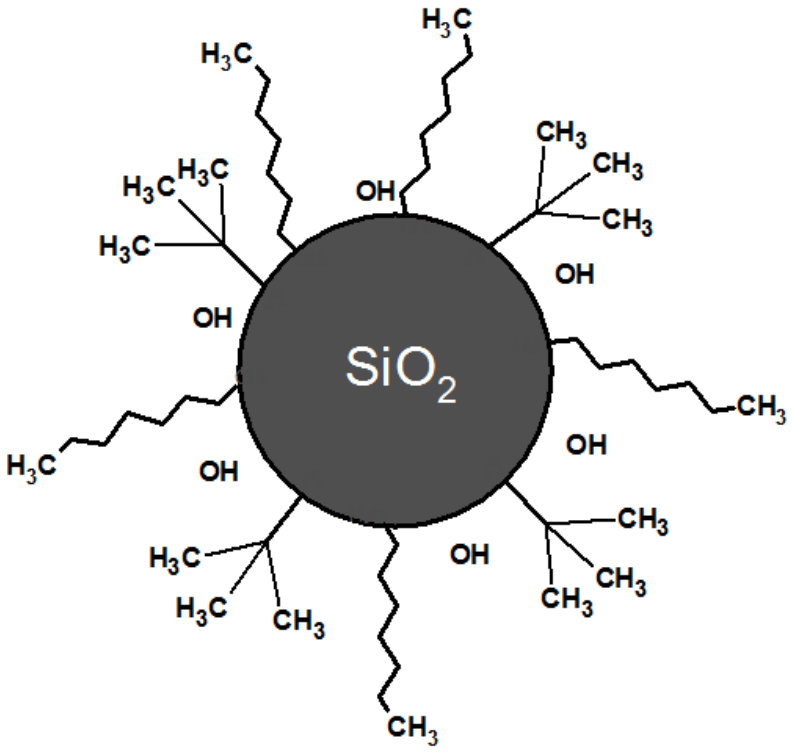

Figure 3.3 Silylated silica-octyl nanoparticle structure.

Silylated silica-anthracene nanoparticles have anthracene, trimethylsilane and residual silanol groups on their surface. Due to the steric hindrance between silanol groups, it is difficult to introduce large functional groups like anthracene to group on silica particles surface. Thus the coverage is lower than the coverage of silylated silica nanoparticles and silylated silica-octyl nanoparticles. From TGA analysis, the anthracene groups are 0.2 mmol/g and the trimethylsilane groups are 0.4 mmol/g. There are 7 anthracene groups (-$C_{18}H_{17}S$), 20 trimethylsilane groups (-$Si(CH_3)_3$) and 70 to 110 -OH groups on individual particle surfaces. The structure of silylated silica-anthracene nanoparticles is shown in Figure 3.4.

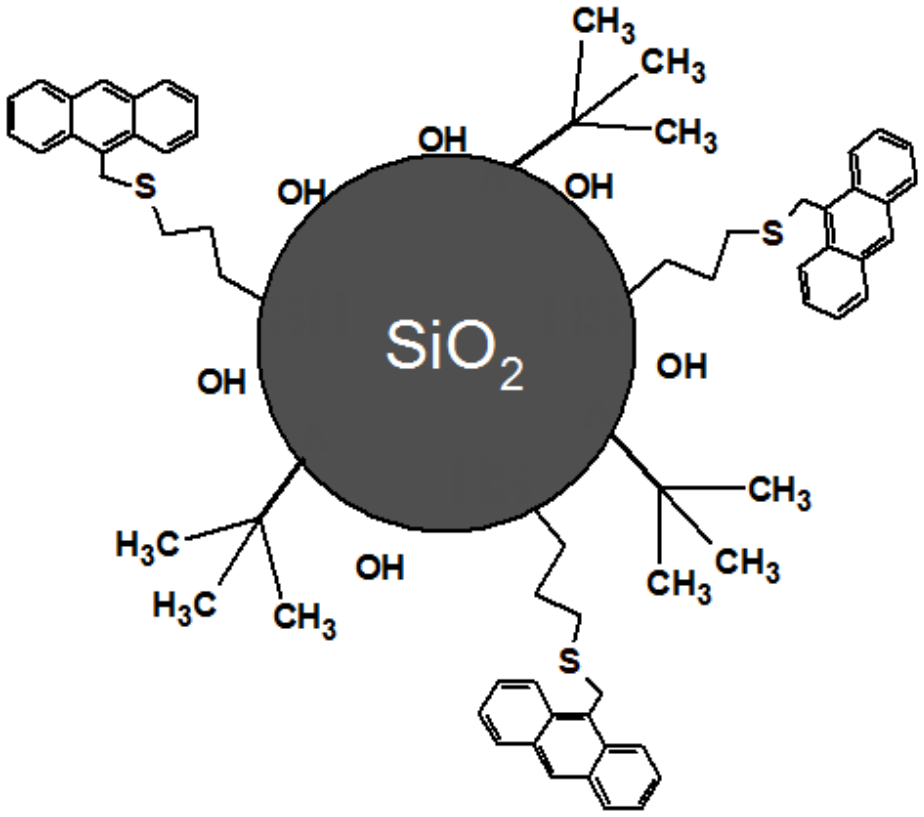

Figure 3.4 Silylated silica-anthracene nanoparticle structure.

3.4 Interfacial Tension Sample Preparation

Silica and functionalized silica nanoparticles are dispersed in pure toluene or heptane + toluene mixtures and sonicated for 30 min at 22 °C. Compositions were set and controlled gravimetrically. The resolution of the balance for nanoparticle mass is 0.1 mg and the uncertainty of mixture compositions is $\pm$0.1 mg for nanoparticles. For the

toluene + heptane mixtures the uncertainty is ±0.1 mL. Samples were used within one day to avoid potential impacts of contamination, aggregation and other artifacts. This phase comprised the internal (drop) phase in the interfacial tension measurements. As the internal phase comprised 2.5 mL this means that the composition uncertainty is 4 % for toluene and heptane, which can make a slight difference in the density data used in interfacial tension (IFT) calculation The aqueous phase (Milli-Q water processed using a Thermo Scientific Lab Water Purification system) was also prepared gravimetrically. The compositions of the acidic, alkaline and salt solutions, prepared using a balance with an uncertainty of 0.001 g. These solutions comprised the external phase in interfacial tension measurements.

3.5 pH Measurement

A Fisher Accumet XL 200 pH/ Conductivity Benchtop Meter, with a resolution of 0.001 pH, was used for pH measurements. The meter contains two parts, a glass probe and a display. The glass probe is made of one pH-responsive electrode, which acts as a sensor, and a reference electrode.[6] The pH values come from the potential difference between the two electrodes, which is determined by the exchange of hydrogen ions in the solution.[5] The pH meter was calibrated with buffer solutions before measurements. For each condition, three measurements were obtained and the reported uncertainty is less than ± 0.1 pH.

3.6 Interfacial Tension Measurements

Options to measure the interfacial tension between two immiscible liquids include: the Du Nouy ring, the Wilhelmy plate, the drop volume, the spinning drop and the pendant drop methods. All have advantages and disadvantages. The method used in this work is the pendant drop method. It is well developed, fast, convenient and accurate.

3.6.1 Pendant Drop Method for Interfacial Tension Measurement

Two immiscible phases are involved in this method. One liquid is contained in a drop. The other phase (the external phase) can be air or a liquid. When the density of the phase in the drop is less than the density of the external phase, the case for this work, a U-shaped needle is needed to hold the drop in place. The arrangement is shown in Figure 3.5. The interfacial tension is determined from the curvature of the drop and the pressure difference across the interface using the Young-Laplace equation:

$$\Delta P = P_{in} - P_{out} = \gamma \left(\frac{1}{R_1} + \frac{1}{R_2} \right) \tag{3.1}$$

Where ΔP is the pressure difference, P_{in} is the pressure inside the droplet, P_{out} is the pressure outside the droplet, γ is the interfacial tension between two phases, R_1 and R_2 are the radii of curvature of the drop. Interfacial tension tends to make the droplet spherical but gravity/buoyancy drags the drop downward/upward. Thus, the drops are pendant-shaped rather than spherical.

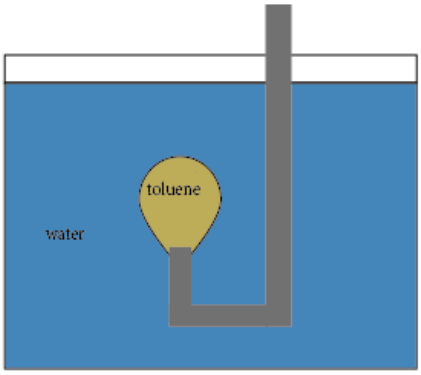

Figure 3.5 Basic setup of two liquid phases (when droplet is the lighter phase).

Drop shape is normally analyzed using images such as the one shown in Figure 3.6. Only half of the drop is shown because drops are normally axisymmetric. R_1 is the radius in the xy plane. R_2 is the radius in the xz plane. A and P are points on the interface which can be picked randomly. P_0 is the pressure at origin point. Both of the pressures are according to Pascal's Law, the hydrostatic pressure between two points of different elevation and can be written as:$\Delta\rho gz$, where $\Delta\rho$ is the

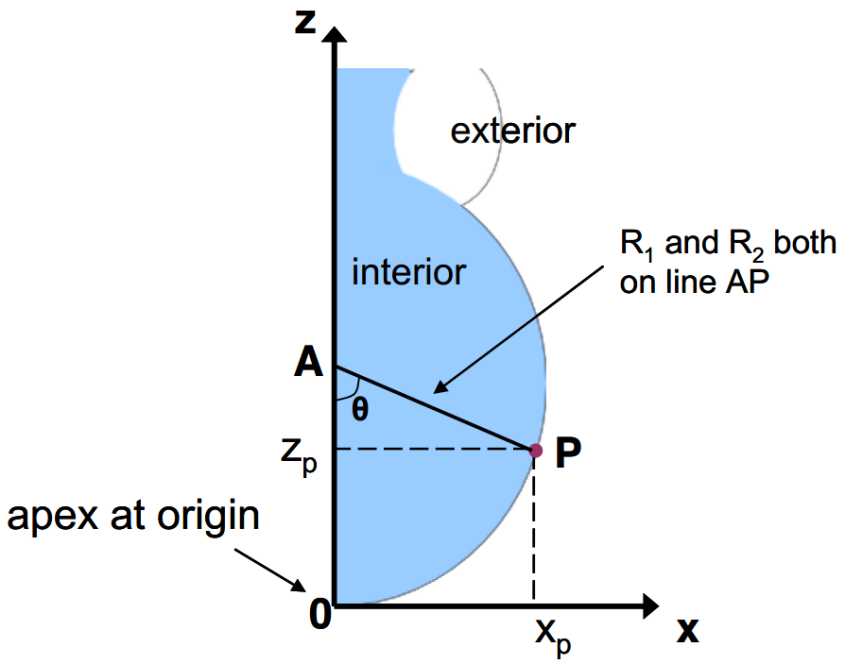

Figure 3.6 Scheme of drop shape analysis.[7]

density difference between two phases and g is the gravitational constant. At the origin,

$$R_1 = R_2 = R \tag{3.2}$$

According to Laplace equation, the pressure difference at origin point is:

$$\Delta P_0 = \frac{2\gamma}{R} \tag{3.3}$$

the pressure difference (ΔP) between point *P* and *z* can be written as:

$$\Delta P_{(z)} = \Delta P_0 \pm \Delta \rho g z \tag{3.4}$$

Where $\Delta P_{(z)}$ is the Laplace pressure at a distance *z* from the plane (x,y,0).Thus, *R* is the radius at the apex. Drop shape analysis process can give interfacial tension values for all

surface points on a drop. As long as drop shape and the density difference between the phases are known, the interfacial tension can be calculated. The pendant drop method is the basis for interfacial tension measurements for the goniometer used in this work.

$$\Delta P = \gamma\left(\frac{1}{R_1}+\frac{1}{R_2}\right) = \frac{2\gamma}{R} \pm \Delta\rho g z \tag{3.5}$$

$$\frac{1}{R_1}+\frac{\sin\theta}{x} = \frac{2}{R} \pm \frac{\Delta\rho g z}{\gamma} \tag{3.6}$$

3.6.2 Interfacial Tension Goniometer

All the interfacial tension measurements in this work were done with a Ramé-Hart goniometer model 250. The goniometer is a powerful tool for measuring contact angle and interfacial tension. It also can also be used for measuring the dilatational rheology of interfaces including dilatational elasticity and viscosity. The equipment setup of the goniometer is shown in Figure 3.7. The setup contains a fiber optical illuminator, a specimen stage that can be adjusted in three dimensions, and a SuperSpeed Digital Camera. The goniometer is connected to a computer for drop shape analysis. DROPimage Advanced serves as the Drop Shape Analyser (DSA) in this system.

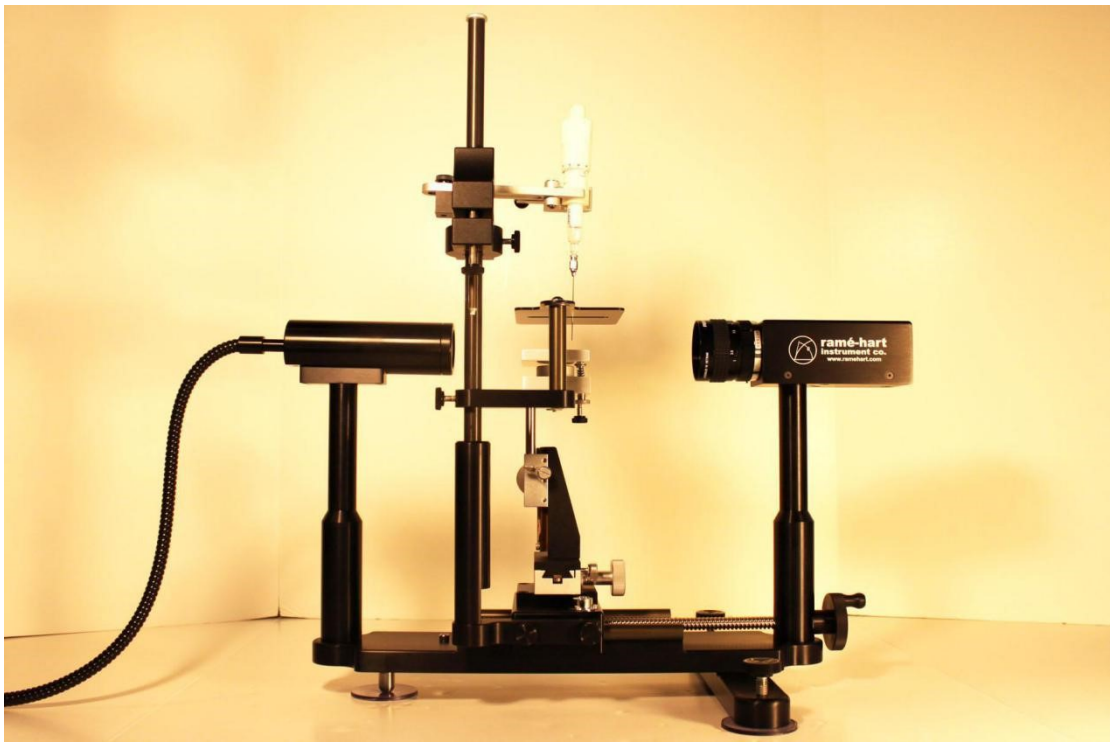

Figure 3.7 Ramé-Hart Goniometer Model 250 Setup.[8]

3.6.3 Interfacial Tension Measurement Procedure

Measurements were performed at 22 °C and atmospheric pressure. The drop phase is held in a microsyringe connected to a needle. There are two types of the needle, a straight needle, which is used when the drop phase is denser than the external phase, and the U-shaped needle, which is used when the drop phase is less dense than the external phase. The external phase is put in a quartz cell, which is then placed on a specimen stage. In this work, in all the measurements a U-shaped needle (22 gauge diameter) was used. The drop is generated at the end of the needle once it is immersed in the external phase. The illuminator lights the experiment area uniformly. The camera captures the curvature of

the drop at 1 frame/s. Images are analyzed using the Drop Shape Analyser (DROPimage Advanced) software. The values of interfacial tension are obtained in real time along with other data such as surface area and drop volume. Every experiment was repeated 3 times to ensure reproducibility. Drop volume can range from 15 to 40 μL and may vary during an experiment. The interfacial tension is calculated by the following equation.

$$\gamma = \left[\Delta\rho g \left(R_0\right)^2 \right] / \beta \tag{3.7}$$

Where γ is the interfacial tension, $\Delta\rho$ is the density difference between the two phases, g is the gravitational constant, R_0 is the radius of curvature at the apex of the drop, β is the shape factor.

3.7 Dynamic Light Scattering

Dynamic Light Scattering (DLS), also called Photon Correlation Spectroscopy, is a powerful method to characterize the size distribution for nano and micro sized particles, emulsions or even molecules. This non-invasive, rapid, convenient and accurate technique is widely used. The theory behind Dynamic Light Scattering derives from the work of John Wiley who found that an electric field induces oscillating polarization of electrons.[10] Molecules and particles in a suspension can shed light and scatter light in an electric field.[10] The size and the shape of particles as well as interactions among them affect the intensity of scattered light. By monitoring the intensity difference between light source (laser 4 mW, 633 nm) and the scattered light, information on the particle size distribution can be obtained.[9] The technique exploits both Brownian motion and the

Doppler shift effect. Brownian motion is described with a probability density function equation:

$$P(r,t) = (4\pi Dt)^{-3/2} \exp(-r^2 / 4Dt) \tag{3.8}$$

Where P is the position of particle, t is time, D is the diffusion constant.

If we assume that the particles are spherical and that they are larger than the solvent molecule/particle radius, then Brownian motion can be described with the Stokes-Einstein equation:

$$D = k_B T / 6\pi\eta a \tag{3.9}$$

Where D is the translational diffusion constant, k_B is the Boltzmann constant, T is the temperature in Kelvin, η is the viscosity of the solvent, a is the hydrodynamic radius of particles. Here particles are considered as spherical in shape. Temperature is needed and has to be stable during the measurement because the viscosity of solvent is closely related to the temperature, which has an impact on the Brownian motion of particles.

Brownian motion is usually slower for smaller particles. In addition, larger particles also exhibit a smaller Doppler shift (a shift in wavelength depends on the relative motion of the source and the observer). The incident beam is scattered by particles undergoing Brownian motion in the suspension.[10] The smaller the particles, the further they can travel in the solvent. To describe the velocity of Brownian motion, translational diffusion coefficient is introduced into the system. The translational diffusion coefficient can be

influenced by many factors including the concentration of particles, the particles themselves and their surface structure. If the solvent is water, the ions in the aqueous phase will also have an impact. The diffusion constant can be obtained from the intensity of scattered light. Thus the hydrodynamic radius of particles can be calculated from the translational diffusion coefficient by the Stokes-Einstein equation. The hydrodynamic radius is measured for a particular system, which is related to both the particles and the solvent used in the system. In other words, when the solvent is changed, for the same particles, the hydrodynamic diameter will also change accordingly. Note that equation (3.9) can only be applied to single scattered light. For multiple scattering 3D cross-correlation method is utilized.

The Dynamic Light Scattering measurements were performed on a Zetasizer Nano ZSP which can be used for both DLS measurement and Zeta potential measurements. Like most DLS equipment, it contains a monochromatic laser light source which lights up the sample in a quartz cell. The scattered light is detected by a digital correlator. The size distribution of particles can be obtained from the fluctuation in scattered light intensity within 3 minutes. The uncertainty of measurements is less than 1 nm. Figure 3.8 shows the basic setup of a dynamic light scattering measurements where the scattered light is collected at an angle of 90°. The scattered light can be collected by the collector at 90° or 173°.[11] The molecules/particles in the suspension scatter light in all directions. On the screen, the speckle pattern can be seen as small dots which stand for the scattered light beams. In Figure 3.7, the black circle stands for the screen, and the white dots stand for

the scattered light beams on the screen. The brighter the area the stronger the light intensity is.

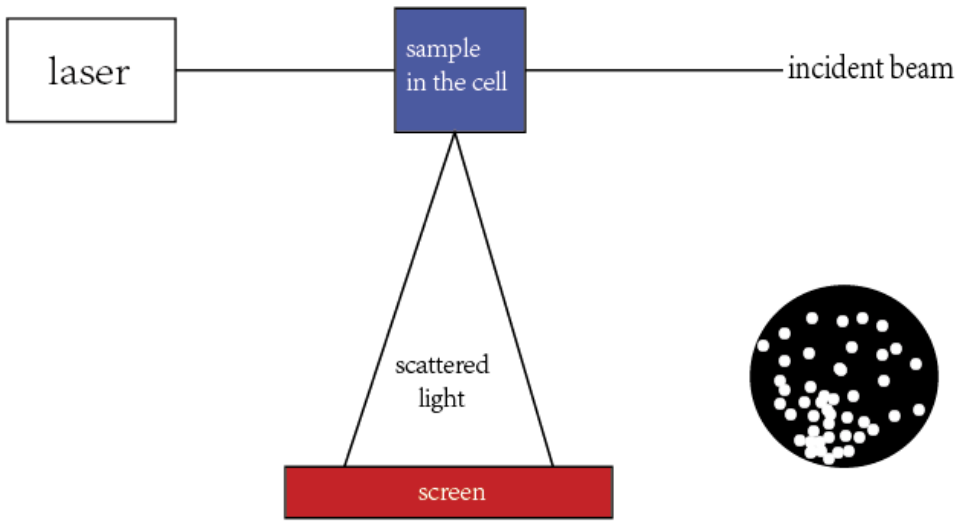

Figure 3.8 Dynamic light scattering schematic.

In real measurements, the screen is replaced by a digital auto correlator which makes it simpler and more efficient to obtain the light intensity than observation of the spectrum. It can compare the two signals or just monitor the change in one single signal. The correlator relates the size of particles with scattered light intensity by a correlation function.

$$\mathrm{G}(\tau) = \langle I(t).I(t+\tau) \rangle \qquad (3.10)$$

Where I is the intensity of scattered light, τ is the time difference between the two signals, G is the correlation function. For monodispersed system, G is an exponential decaying function of time difference τ.

$$\mathrm{G}(\tau) = A[1 + Bexp(-2\Gamma\tau)] \tag{3.11}$$

$$\Gamma = \mathrm{D}q^2 \tag{3.12}$$

$$\mathrm{q} = (4\pi n/\lambda_0)sin(\theta/2) \tag{3.13}$$

Where A is the baseline of the correlation function, B is the intercept of the correlation function, Γ is the decay rate, D is the translational diffusion coefficient, q is the magnitude of the scattering vector, n is the refractive index of solvent, λ_0 is the wavelength of laser, θ is the scattering angle.

When the translational diffusion coefficient is obtained, the hydrodynamic diameter of particles in dispersion can be obtained through the Stokes-Einstein equation.

3.8 Fourier Transform Infrared Spectroscopy

Fourier transform infrared spectroscopy (FTIR) is used in this work to characterize functional groups on nanoparticle surfaces.[12] Monochromatic infrared light is passed through a sample. The output, detected on a pyroelectric detector which can detect the change in temperature as the intensity of infrared light, comprises a wave number spectrum. Peaks in the spectra are characteristic of particular functionalities. All

measurements were performed using a Nicolet™ iS™ 50 FT-IR Spectrometer from Thermo Fisher Scientific with a spectral range is 15,000-27,000 cm^{-1}.

Figure 3.9 shows the basic setup of FTIR. The setup of FTIR mainly includes an IR source, a sample stage, an interferometer, a detector and computer.[12] IR radiation comes out from the source and part of it will be adsorbed by the sample and the rest will pass through the sample and be analysed.[13] However, the whole process takes place far too quick for capture and analysis. Thus, an interferometer is introduced into the system to slow down the process. The interferometer includes of a beam splitter which separate the IR beam in two beams. One of the beams heads towards a fixed mirror, and the other heads towards a moving mirror. The two light beams reflected by the two mirrors will go back into the beam splitter.[14] At the beam splitter, the beams from the two mirrors recombine into one beam and go through the sample and then strike the detector. The two beams of light are not always in phase because one of the mirrors is moving, which mean they can interfere constructively or destructively. The signal of light from the two mirrors is recorded in the interferogram, including the different frequency and the intensity of IR.

After that, the interferogram is converted by Fourier Transform algorithm which transfers it in to a spectrum that includes the information on adsorption, emission and transmission. The process is done by the computer and the spectrum is ready for the analysis later.

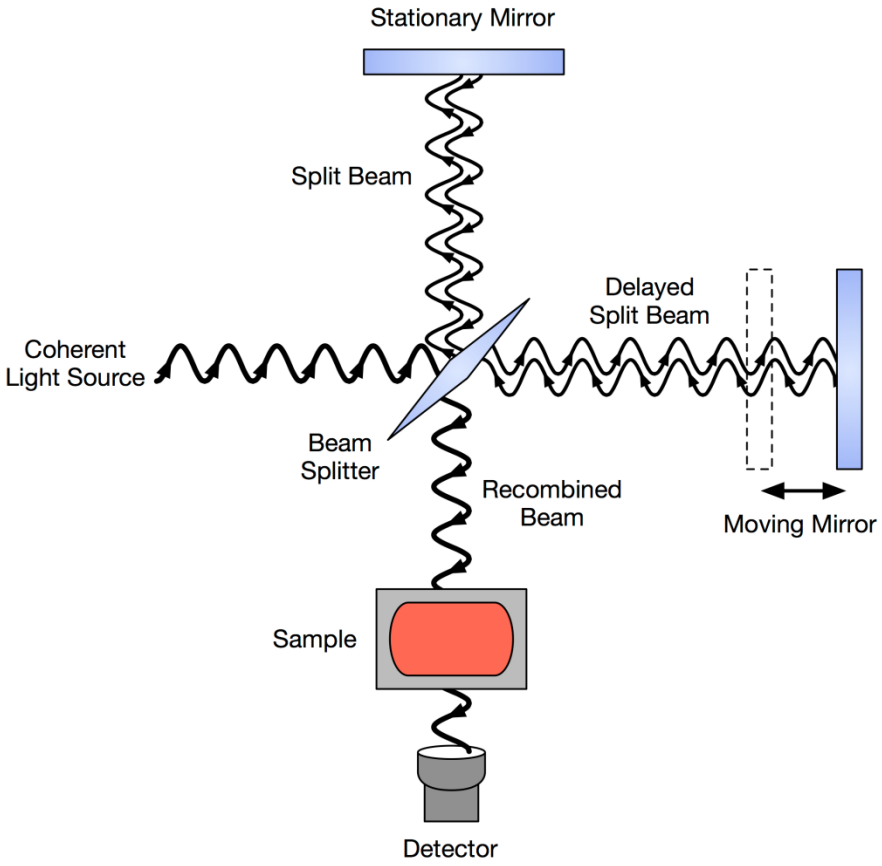

Figure 3.9 FTIR setup schematic.[15]

3.9 References

(1) Calero, P.; Martínez-Máñez, R.; Sancenón, F.; Soto, J. Synthesis, Characterisation and Optical Properties of Silica Nanoparticles Coated with Anthracene Fluorophore and Thiourea Hydrogen-Bonding Subunits. *European Journal of Inorganic Chemistry* **2008***, 2008*, 5649-5658.

(2) Montalti, M.; Prodi, L.; Zaccheroni, N.; Falini, G. Solvent-Induced Modulation of Collective Photophysical Processes in Fluorescent Silica Nanoparticles. *J. Am. Chem. Soc.* **2002***, 124*, 13540-13546.

(3) Badiei, A.; Bonneviot, L.; Crowther, N.; Ziarani, G. M. Surface Tailoring Control in Micelle Templated Silica. *Journal of organometallic chemistry* **2006***, 691*, 5911-5919.

(4) Kahaniani, Y.; Shaw, J. M. Characterization and Shear Rheology of Silica Nanoparticles Functionalized with Alkyl and Alkyl-Aromatic Ligands. Internal Report 2014, 13.

(5) Cerveny, S.; Schwartz, G. A.; Otegui, J.; Colmenero, J.; Loichen, J.; Westermann, S. Dielectric Study of Hydration Water in Silica Nanoparticles. *The Journal of Physical Chemistry C* **2012***, 116*, 24340-24349.

(6) PragoLab In *pH Measurement Handbook * Thermo Scientific, Inc.: 2017;2-4.

(7) Kumar, B. Effect of Salinity on the Interfacial Tension of Model and Crude Oil Systems, University of Calgary, 2012.

(8) Carl Clegg Ramé-Hart Goniometer Model 250 Pictures. *https://www.flickr.com/photos/51015268@N07/sets/72157634050986433/*.

(9) Jian, C.; Poopari, M. R.; Liu, Q.; Zerpa, N.; Zeng, H.; Tang, T. Reduction of Water/Oil Interfacial Tension by Model Asphaltenes: The Governing Role of Surface Concentration. *The Journal of Physical Chemistry B* **2016***, 120*, 5646-5654.

(10) Berne, B. J.; Pecora, R. In *Dynamic light scattering: with applications to chemistry, biology, and physics;* Courier Corporation: 2000; 10-45.

(11) Washington, C. In Particle Size Analysis In Pharmaceutics And Other Industries: Theory And Practice: Theory And Practice; CRC Press: 2005;101-106 .

(12) Griffiths, P. R.; De Haseth, J. A. In *Fourier transform infrared spectrometry;* John Wiley & Sons: 2007; Vol. 171.

(13) Saptari, V. In Fourier transform spectroscopy instrumentation engineering; SPIE press: 2004; Vol. 61.

(14) Korb, A. R.; Dybwad, P.; Wadsworth, W.; Salisbury, J. W. Portable Fourier Transform Infrared Spectroradiometer for Field Measurements of Radiance and Emissivity. Appl. Opt. 1996, 35, 1679-1692.

(15) Sanchonx Interferometer for FTIR. https://commons.wikimedia.org/wiki/File:FTIR_Interferometer.png.

CHAPTER 4: RESULTS AND DISCUSSION

Results obtained from FTIR characterization, DLS measurements and interfacial tension measurements of samples are provided and discussed in this chapter. The interfacial tension measurement results show the effect of particle concentration, water pH and water salinity. The FTIR characterization regarding the surface structure of functionalized silica nanoparticles, the subject of an internal report prepared by Yeganeh Khaniani is also included in this chapter. The size distribution of silylated silica-anthracene nanoparticles in toluene was characterized by dynamic light scattering.

4.1 FTIR Characterization of Silica Nanoparticles

The silica nanoparticle samples are in powder. A small amount of powder is put on the exposed top area of ATR crystal using a spatula. The pressure arm is adjusted until it just touches the sample. The silica nanoparticle samples were characterized by FTIR. Figure 4.1 shows the FTIR spectra of functionalized silica nanoparticles performed by Yeganeh Khaniani.[1] The Si-O bands are reflected by the adsorption peaks at 1100 cm^{-1} and 810 cm^{-1}. The small adsorption peaks at 2900 cm^{-1} stands for trimethylsilane ($-Si(CH_3)_3$) groups. The aromatic rings are represented by the small adsorption peaks at 1520 cm^{-1} and 1380 cm^{-1}.

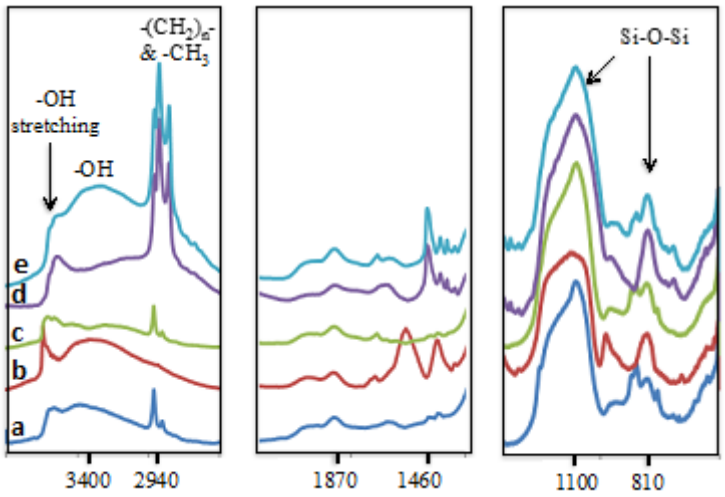

Figure 4.1 FTIR spectra of (a) silylated silica, (b) silica-anthracene, (c) silica-anthra-silyl, (d) silica-octyl and (e) silica-octyl-silyl.[1]

4.2 DLS Characterization

The aggregation of nanoparticles is an important phenomenon that impacts their interfacial behavior and their colloidal suspension stability. Not all aggregates can be captured by DLS methods. Some aggregates are too small or their concentration too low to be detected by DLS. Figure 4.2 shows the size distribution for 500 mg/L silylated silica-anthracene nanoparticles in toluene dispersion. The small peak at 7.3 nm reflects the size of single silylated silica-anthracene nanoparticles, whereas, the high intensity peak at 214.4 nm indicates the presence of aggregates. More information about this measurement was in the appendix. For silylated silica and silylated silica-octyl nanoparticles in toluene, the DLS failed to characterize the size distribution. However, it

was observed that there were aggragetes at the bottom of container for both particle suspensions.

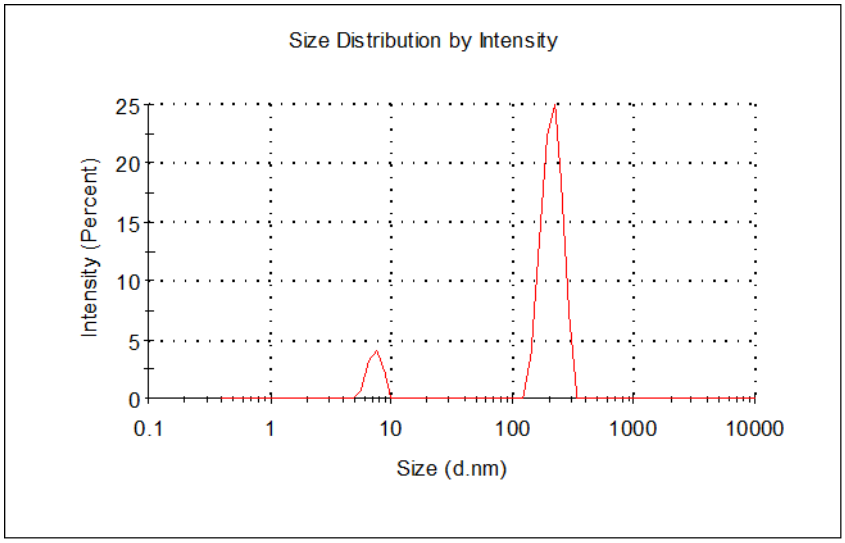

Figure 4.2 Size distribution for 500 mg/L silylated silica-anthracene nanoparticles in toluene suspension.

4.3 Interfacial Tension Measurements

Interfacial tension measurements were conducted to investigate the effect of particle surface properties and concentration, aqueous phase pH and salinity on interfacial tension. Calculating the interfacial tension between two phases requires the density values of both the phases. The densities of the hydrocarbon solvents used in the calculations were obtained from the NIST Chemistry Webbook[2] and are listed in **Table 4.1.**

Table 4.1 Density (at 23°C) of solvents used in this work.[2]

Solvent Name	**Density (g/cm^3)**
Toluene	0.867
Heptane	0.684
Heptane+ toluene (volume ratio 50:50)	0.775
Water	0.999

Functionalized silica nanoparticles were dispersed in toluene (the droplet phase) with water as the external phase. Interfacial tension measurements were taken every second for 1800 seconds for samples with nanoparticle concentrations ranging from 100 mg/L to 500 mg/L. The silica nanoparticles did not readily dispersed in toluene at higher concentrations. Interfacial tension measurement uncertainties of less than $\pm$0.25mN/m were achieved, at 23°C and under atmospheric pressure, based on 3 successive measurements for time dependent values. Equilibrium interfacial tension values comprise averages of the last 200 interfacial tension measurements in a series of measurements.

4.3.1 Effect of Particle Concentration on Interfacial Tension

As noted in Chapter 2, section 2.73, the energy required for nanoparticles to adsorb on an interface is usually larger than the thermal energy (kT). Therefore, the adsorption of nanoparticles may be assumed to be irreversible.[3] The attachment energy of particles is a function of their radius. This is different from surfactant molecules. For most molecular surfactants adsorption is reversible.[4] For interfaces and molecular surfactants, adsorption kinetics are also typically faster. Below the critical micelle concentration (CMC), increasing the concentration of surfactants usually decreases interfacial tension. Above the CMC, no further adsorption occurs and surfactant molecules form micelles in the bulk instead of adsorbing on the interface. For interfaces with colloidal particles, adsorption kinetics is related to the size and shape of the particles. Colloidal particles also tend to aggregate in the bulk at higher concentrations and the suspension may become unstable.

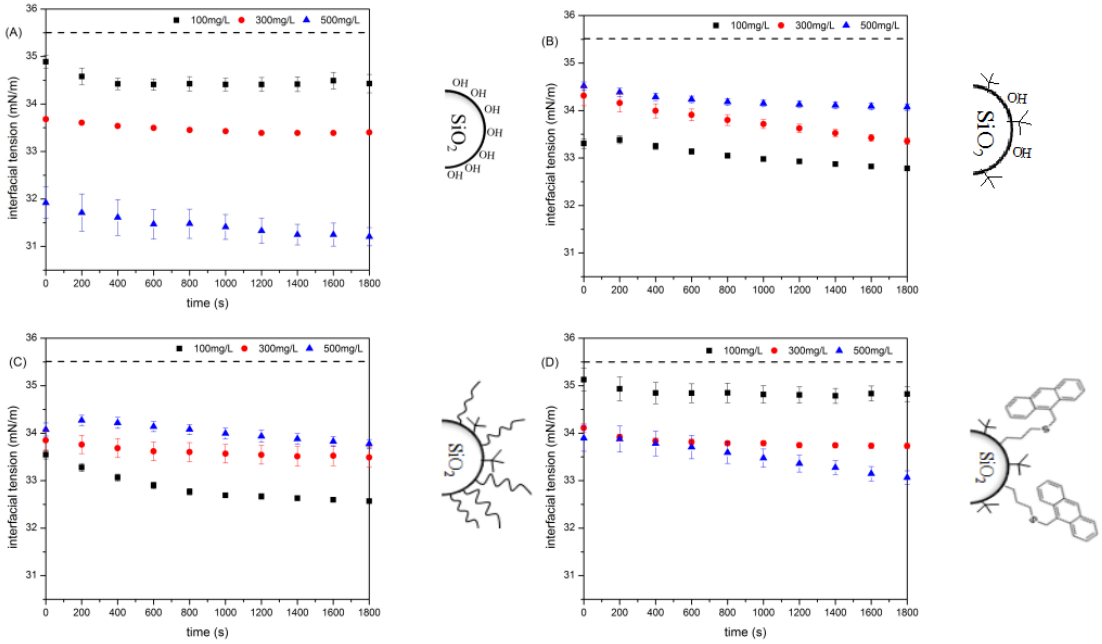

Figure 4.3 Interfacial tension between water and silica nanoparticles in toluene suspension at nanoparticle concentrations of 100 mg/L, 300 mg/L, 500 mg/L; (A) silica nanoparticles; (B) silylated silica nanoparticles; (C) silylated silica-octyl nanoparticles; (D) silylated silica-anthracene nanoparticles; the dash line stands for the interfacial tension between water and pure toluene, measured at 23°C and atmospheric pressure.

In Figure 4.3 (A), at 500 mg/L, the effect of silica nanoparticles on the interfacial tension value is apparent. The interfacial tension dropped to around 31 mN/m after 1800 seconds which is the lowest equilibrium interfacial tension that can be achieved in this set of experiments. These particles have less impact at lower concentrations and below 100 mg/L their effect is insignificant.

The interfacial tension measurement results for silylated silica-anthracene nanoparticles suspensions are shown in Figure 4.3(D). Similar to bare silica nanoparticles, the silylated silica-anthracene nanoparticles behave like most surfactants below CMC. The interfacial tension decreases at higher concentration. The effect of silylated silica-anthracene nanoparticles at 100 mg/L interfacial tension is negligible. The interfacial tension decreases to around 33 mN/m at 500 mg/L. Compared with bare silica nanoparticles, the silylated silica-anthracene nanoparticles are less effective at 500 mg/L. The anthracene ligands at the surface of silica nanoparticles can aggregate due to π-π stacking which is one possible reason why they are less effective than bare silica nanoparticles.

The dynamic interfacial tension of silylated silica and silylated silica−octyl nanoparticle suspension is shown in Figure 4.3(B) and 4.3(C), respectively. Both the silylated silica nanoparticles and silylated silica-octyl nanoparticles are functionalized with aliphatic chains and they behave in a similar way. The effect of concentration of both these particles on interfacial tension is opposite to that of silica nanoparticles, i.e. at higher concentrations, the reduction in interfacial tension is smaller than at low concentration. At higher concentrations, both silylated silica and silylated silica-octyl nanoparticles tend to aggregate and therefore they become less effective in lowering the interfacial tension. Large aggregates require more energy to adsorb on the interface than smaller ones and must overcome gravity to adsorb on the interface. It was observed that some aggregates also settled at the bottom of the drop in some high concentration experiments. Among the two types of nanoparticles, silylated silica-octyl nanoparticles were slightly more effective than the silylated silica nanoparticles.

4.3.2 Effect of aqueous phase pH on Interfacial Tension

Interfacial tension can be affected by the pH of the aqueous phase. The four types of silica nanoparticles were dispersed in heptane + toluene (volume ratio 50:50) with the concentration of 300 mg/L. Based on the experiments on the effect of particle concentration section 4.3.1, functionalized silica nanoparticles aggregate in toluene. With the addition of heptane as a solvent, the functionalized silica nanoparticles are better dispersed. The suspensions were sonicated for 30 minutes to ensure that the nanoparticles were well dispersed. Six pH values were chosen in the pH range 2 to 12 (both inclusive) for studying the effect of pH on interfacial tension. pH was adjusted by adding hydrochloric acid (HCl) and sodium hydroxide (NaOH). The pH values of solutions were measured using a pH meter. The uncertainty in pH measurements was within 0.1 pH unit. For this study, the nanoparticle suspensions were the droplet phase and water with different pH was the external phase. Interfacial tension measurements were made every second for 1800 seconds.

In the absence of nanoparticles, the interfacial tension between water with pH around 5.6 and heptane + toluene (volume ratio 50:50) is 41mN/m.[5] This is the reference line in Figure 4 A-D. Figure 4.4(A) shows the dynamic interfacial tension between suspensions of silica nanoparticles and water at different pH values. In alkaline environments, hydroxide ions are abundant in the aqueous phase. Both the hydroxide ions and silica nanoparticles can adsorb on the oil/water interface and lower the interfacial tension. The silica nanoparticles on the interface carry negative charges, which can be neutralized by

the cations in the aqueous phase. Thus, the repulsive interaction between nanoparticles could be weakened, which allow a higher surface excess concentration on the oil/water interface. According to adsorption isotherms, higher the surface excess concentration (before saturation) is, lower the equilibrium interfacial tension. Figure 4.4(B) shows the dynamic interfacial tension between suspension of silylated silica nanoparticles and water of different pH values. The lowest equilibrium interfacial tension under different pH for silylated silica nanoparticle suspension is around 32 mN/m. The effect of pH is insignificant up to pH=8. Compared with silica nanoparticles, the silylated silica nanoparticles are more effective at lowering the interfacial tension between water and heptane + toluene (volume ratio50:50), especially in highly alkaline environment. Figure 4.4(C) shows the dynamic interfacial tension between suspension of silylated silica-octyl nanoparticles and water of different pH values. The effect of silylated silica-octyl nanoparticles is similar to silica nanoparticles. Like silica nanoparticles and silylated silica nanoparticles, the reduction in interfacial tension reached minimum when pH is around neutral. Figure 4.4(D) shows the dynamic interfacial tension between suspension of silylated silica-anthracene nanoparticle suspension and water of different pH values. The lowest equilibrium interfacial tension for silylated silica-anthracene nanoparticle suspension is around 36 mN/m, which is observed at pH=12. At all other pH, except for pH=8, the equilibrium interfacial tension is around 39mN/m. The reduction in interfacial tension is the minimum at pH=8. At pH=12, the abundant cations in the aqueous phase can neutralize the negative charge on nanoparticle surface to the most extent, which allows the highest surface excess concentration on the interface. The dynamic interfacial

tension of silylated silica-anthracene nanoparticles, also reaches a steady state after 600 seconds for different pH.

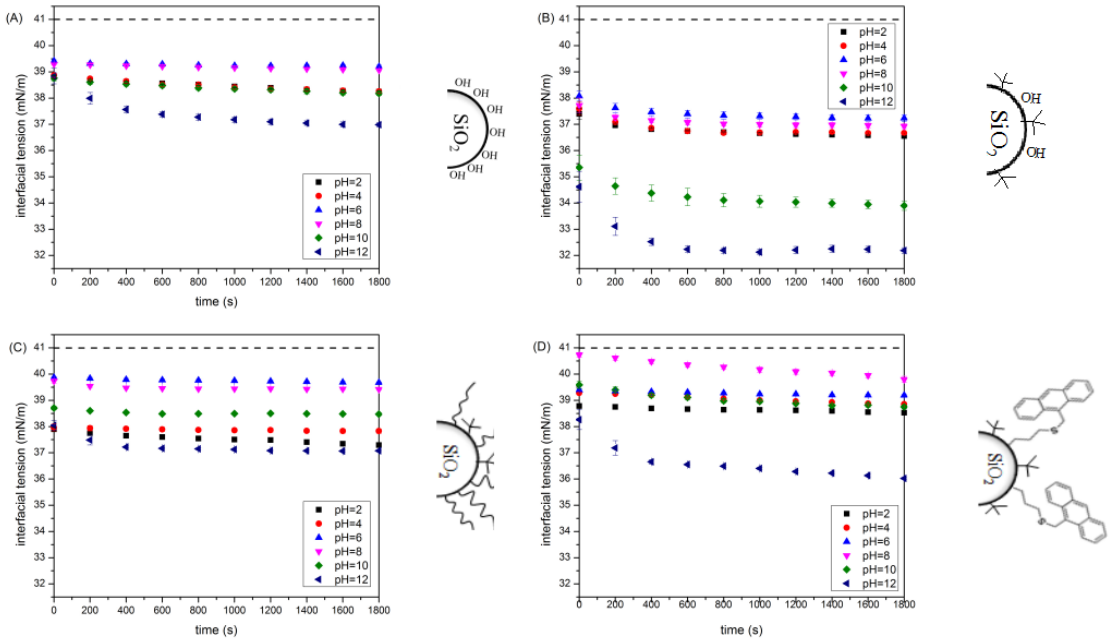

Figure 4.4 Interfacial tension between water of different pH and silica nanoparticles suspended in heptane + toluene (volume ratio 50:50) mixture at 300 mg/L; (A) silica nanoparticles; (B) silylated silica nanoparticles; (C) silylated silica-octyl nanoparticles; (D) silylated silica-anthracene nanoparticles; the dash line stands for the interfacial tension between water and heptane + toluene mixture (volume ratio 50:50), measured at 23°C and atmospheric pressure.

Among all the four types of nanoparticles, silylated silica nanoparticles are most effective in reducing the interfacial surface tension at pH=12. The possible reason of this might be that silica nanoparticles (both functionalized and non-functionalized) used in the measurements carry negative charge on the surface. In a highly alkaline environment, the

abundant cations in the aqueous phase neutralize the surface charge of nanoparticles on the interface. With less negative surface charge, the nanoparticles can reach a higher surface excess concentration on the interface, which makes them more effective at very high pH.

Equilibrium interfacial tension values for all four nanoparticle suspension types at different pH values are shown in Figure 4.5. For the four samples the curves of interfacial tension are all bell-shaped, this is in agreement with most studies focusing on the interfacial tension between crude oil and water system. It is also clear that silylated silica nanoparticles are more effective than the other three types.

For emulsion breakage, neutral pH is favored. Higher interfacial tension makes it easier to break the emulsion. Lower surface excess of particles leads to lower mechanical strength of the interface.

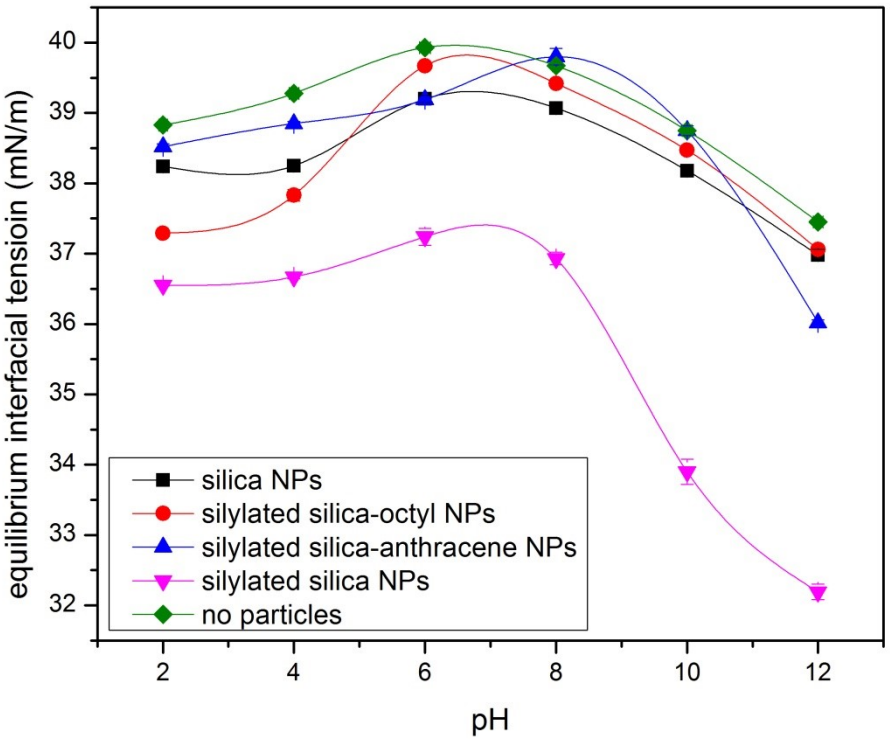

Figure 4.5 Cross plot of Interfacial tension between water of different pH and silica nanoparticles suspended in heptane + toluene (volume ratio 50:50) mixture at 300 mg/L, measured at 23°C and atmospheric pressure.

The higher effectiveness of silylated silica nanoparticles may be due to the trimethylsilane ($-Si(CH_3)_3$) on the particle surface, which is smaller in size compared with octyl functional groups. The trimethylsilane ($-Si(CH_3)_3$) give rise to steric repulsion between nanoparticles but the steric repulsion is smaller than that between silylated silica-octyl nanoparticles considering their longer chain. Thus, this kind of steric repulsion can prevent the nanoparticles from aggregation but will not hinder the increase

of surface excess concentration which explains why the silylated silica nanoparticles are more effective than the other three samples.

4.3.3 Effect of aqueous phase salinity on Interfacial Tension

Water salinity can impact the interfacial tension between water and organic phases or organic phases + surfactants. Interfacial tension generally increases with an increase in salinity[6] but when surfactants or solid particles are present, the change in interfacial tension is variable. [7]To study the effect of aqueous phase salinity on interfacial tension, all the four types of silica nanoparticles were dispersed in heptane + toluene (volume ratio 50:50), with a concentration of 300 mg/L. Two types of salts were used for this study: NaCl and $CaCl_2$. The dynamic interfacial tension of samples was measured every second for 1800 seconds. The concentration of salt was 1 mM, 10 mM and 100 mM. The measurements were carried out at 23°C and atmospheric pressure.

Figure 4.6(A) shows the dynamic interfacial tension between silica nanoparticle suspension and NaCl water solutions. The dynamic interfacial tension for samples with1 mM and 10 mM NaCl solution is almost same. The equilibrium interfacial tension is around 39 mN/m. At salt concentration of 100 mM, there is an obvious change in the dynamic interfacial tension. The interfacial tension starts from 35 mN/m and finally reaches around 32.5 mN/m at equilibrium. There is no noticeable change in the slope of curves when the NaCl concentration is 1 mM or 10 mM. For 100 mM solution, the slope of interfacial tension curve drops rapidly in the first 600 s, which means the adsorption

process happens rapidly at the start. As the surface excess concentration on the interface approaches saturation, the speed of adsorption decreases. Figure 4.6(B) shows the dynamic interfacial tension between silylated silica nanoparticle suspension and NaCl water solutions. When the concentration of NaCl solution is 1 mM, the equilibrium interfacial tension is around 38.5 mN/m. The equilibrium interfacial tension is about 37.25 mN/m and 36.75 mN/m, respectively, when the NaCl concentration is 10 mM and 100 mM. Compared with silica nanoparticles when the NaCl concentration is 100 mM, the silylated silica nanoparticles are less effective at reducing IFT. Different from silica nanoparticles, there is an obvious change during the first 400 seconds of the measurements in the slope of dynamic interfacial tension curves under different concentration. Thus the change in the slope of dynamic interfacial tension can be observed in this period. The rate of adsorption slows down after 400 seconds. Figure 4.6(C) shows the dynamic interfacial tension between the silylated silica-octyl nanoparticle suspension and NaCl water solutions. When the concentration of NaCl solution is 1 mM, the equilibrium interfacial tension is around 37.0 mN/m, which is more effective than silica nanoparticle and silylated silica nanoparticles. The dynamic interfacial tension curves when NaCl concentration is 10 mM and 100 mM are similar in shape and close to each other, which indicates the change in concentration does not strongly influence the adsorption process when the concentration is higher than 10 mM. The equilibrium interfacial tension under both concentrations is around 35.5 mN/m, which is more effective at lowering the interfacial tension than silylated silica nanoparticles. In the first 400 seconds of the measurements, the interfacial tension drops quickly and slows down afterwards under all the three different concentration. It is

obvious that the change in the slope of dynamic interfacial tension curves is larger under higher NaCl concentration. Figure 4.6(D) shows the dynamic interfacial tension between silylated silica-anthracene nanoparticle suspension and NaCl water solutions. The equilibrium interfacial tension is about 36.2 mN/m and 35.6 mN/m respectively when the NaCl concentration is 10 mM and 100 mM, where the difference in equilibrium IFT is not big. In the first 400 seconds of the measurements, the interfacial tension drops quickly and slows down afterwards under the concentration of 1 mM and 10 mM. When the concentration is 100 mM, the adsorption process slows down after 600 seconds. In addition, the change in the slope of dynamic interfacial tension curves is larger at higher NaCl concentration.

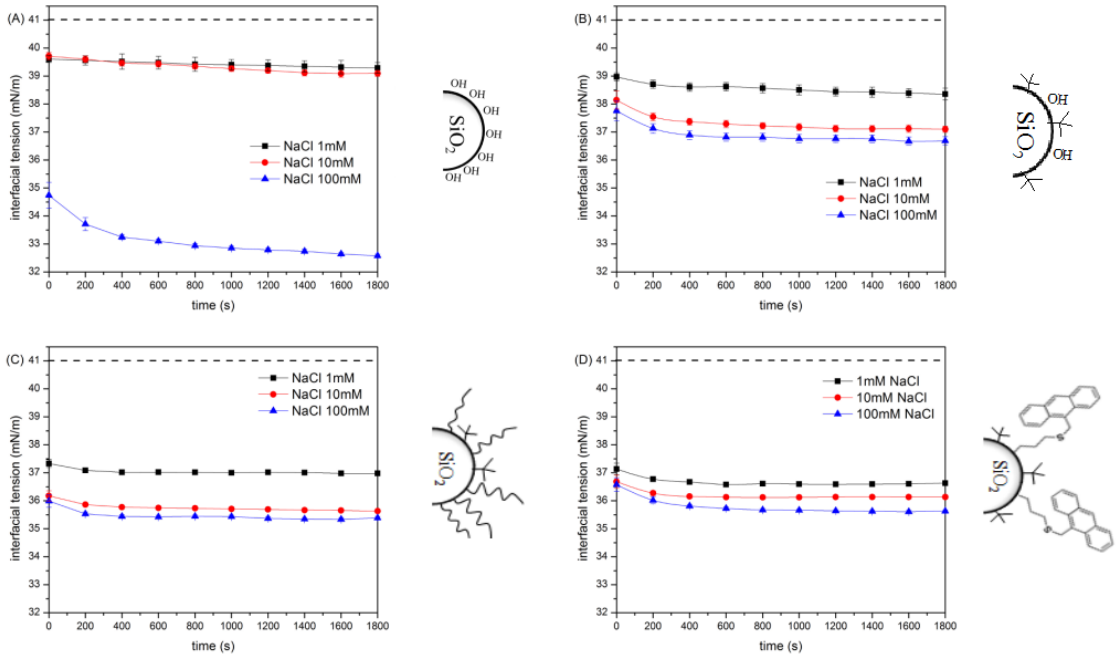

Figure 4.6 Interfacial tension between silica nanoparticle suspension (300 mg/L nanoparticles dispersed in heptane + toluene (volume ratio 50:50) and NaCl water solution of different concentration; (A) silica nanoparticles; (B) silylated silica nanoparticles; (C) silylated silica-octyl nanoparticles; (D) silylated silica-anthracene nanoparticles, the dash line stands for the interfacial tension between water and heptane + toluene mixture (volume ratio 50:50), measured at 23°C and atmospheric pressure.

Figure 4.7(A) shows the dynamic interfacial tension between silica nanoparticle suspension and $CaCl_2$ water solutions. In contrast to NaCl solutions, the dynamic interfacial tension is easily distinguishable for 1 mM and 10 mM, even though the difference is not big. The equilibrium interfacial tension between silica nanoparticle suspension and 1 mM $CaCl_2$ is around 40mN/m. For 10 mM $CaCl_2$, the equilibrium interfacial tension is about 38mN/m. Similar to the cases of NaCl solution, there is no

obvious change in the slope of curves with increasing $CaCl_2$ concentration up to 10 mM. At concentration of 100 mM, the slope of interfacial tension drops rapidly in the first 600 s, which means the adsorption process happens rapidly at the start. As the surface excess concentration on the interface approaches saturation, the speed of adsorption decreases. Figure 4.7(B) shows the dynamic interfacial tension between silylated silica nanoparticle suspension and $CaCl_2$ water solutions. The lowest equilibrium interfacial tension reached in these measurements is around 36.25mN/m. Silylated silica nanoparticles are less effective than silica nanoparticles at reducing IFT under the same conditions. The dynamic interfacial tension curves are very similar in shape when the $CaCl_2$ concentration is 1 mM and 10 mM. The equilibrium interfacial tension is around 38.25 mN/m and 37.50 mN/m, respectively. When $CaCl_2$ concentration goes up to 100 mM, the interfacial tension drops quickly in the first 800 s and then decrease in a rather slow rate. This indicates that under a higher concentration, $CaCl_2$ improves the adsorption process. Thus a clear change in the slope of dynamic interfacial tension curve under the concentration of 100 mM $CaCl_2$ is observed. Figure 4.7(C) shows the dynamic interfacial tension between silylated silica-octyl nanoparticle suspension and $CaCl_2$ water solutions. When the concentration of NaCl solution is 1 mM, the equilibrium interfacial tension is around 37.5 mN/m, which is more effective than silica nanoparticle and silylated silica nanoparticles, but less effective than silylated silica-octyl nanoparticles. Different with silylated silica nanoparticle, the equilibrium interfacial tension between silylated silica-octyl nanoparticles and $CaCl_2$ solution when concentration is 10 mM and 100 mM is about 35.25 mN and 34.5 mN/m respectively, which indicates that changes in concentration above 10 mM do not strongly influence the adsorption process. During the

first 400 seconds of the measurements, the interfacial tension drops quickly and slows down at the concentration of 1 mM and 10 mM. When the concentration is 100 mM, the adsorption process slows down after 600 seconds. In addition, the change in the slope of dynamic interfacial tension curves is larger at higher $CaCl_2$ concentrations. The reason is that more ions can neutralize the surface charge on the surface of silylated silica-octyl nanoparticles which allows a higher surface excess concentration. Figure 4.7(D) shows the dynamic interfacial tension between silylated silica-anthracene nanoparticle suspension and $CaCl_2$ water solutions. When the $CaCl_2$ concentration is 1 mM and 10 mM, the equilibrium interfacial tension is around 38 mN/m, where the dynamic interfacial tension curves are also in similar shape. This shows that Ca^{2+} ions are less effective than Na^+ ions at reducing IFT. The possible reason is that Ca^{2+} ions are larger than Na^+ in size. The radius of hydrated calcium ions is 4.1 Å.[8] For hydrated sodium ions, the radius is 3.6 Å.[8] The anthracene groups on nanoparticle surface can cause aggregation due to π-π stacking interactions which are the attractive interactions commonly between aromatic rings.[9] The surface area is greatly reduced due to the aggregation, which also limit the neutralization of surface charge. The size of hydrated sodium ions is smaller than hydrated calcium ions. It is easier for hydrated sodium ions to get in between the ligands on nanoparticles and inside the aggregates. Thus, the sodium ions are more effective for the surface charge neutralization of silylated silica anthracene nanoparticles. At 1 mM and 10 mM, the adsorption process slows down after 800 seconds. However, when the $CaCl_2$ concentration reaches 100 mM, the shape of dynamic interfacial tension curve changes a lot, which indicates a change in the adsorption dynamics. In the first 400 seconds, the adsorption process is going on quickly which can be observed from the slope

of the curve. After 400 seconds, the adsorption process slows down and continues throughout 1800 seconds, which indicates that the adsorption process last for a longer time than any situation mentioned.

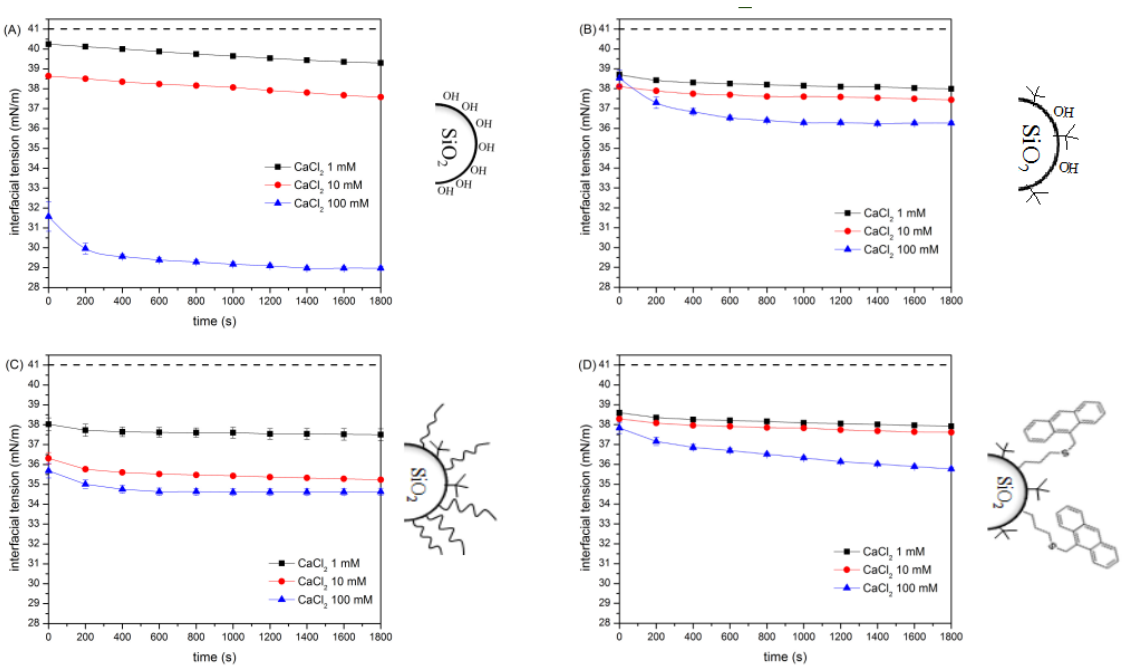

Figure 4.7 Interfacial tension between silica nanoparticle suspension (300 mg/L) nanoparticles dispersed in heptane + toluene (volume ratio 50:50) and $CaCl_2$ water solution of different concentration, (A) silica nanoparticles; (B) silylated silica nanoparticles; (C) silylated silica-octyl nanoparticles; (D) silylated silica-anthracene nanoparticles, the dash line stands for the interfacial tension between water and heptane + toluene mixture (volume ratio 50:50), measured at 23°C and atmospheric pressure.

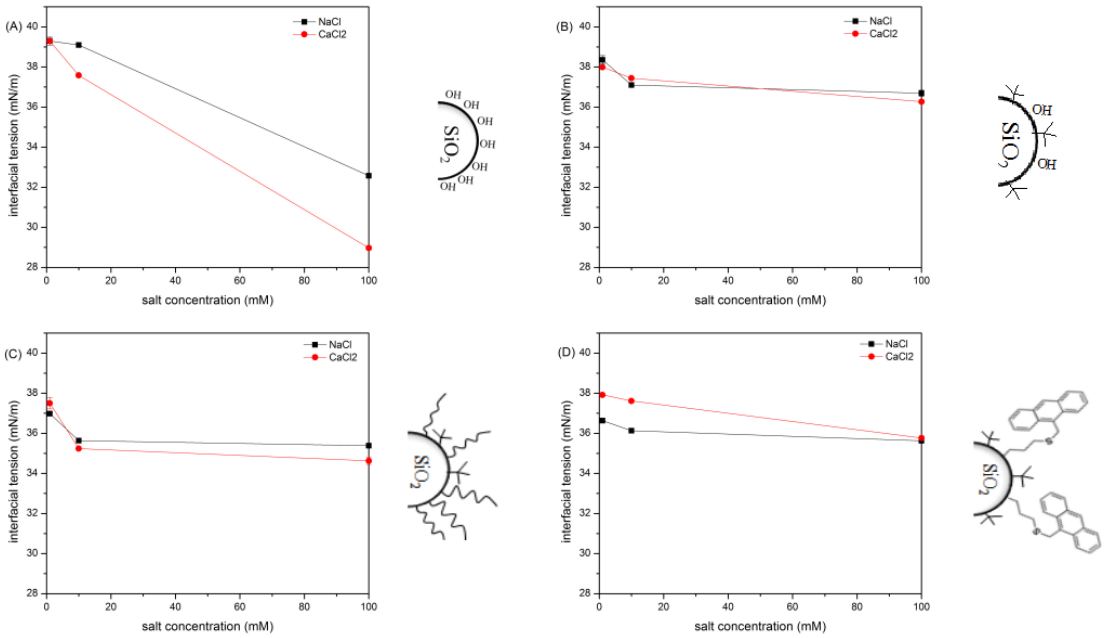

Figure 4.8 Equilibrium interfacial tension between silica nanoparticle suspension and salt solutions, (A) silica nanoparticles; (B) silylated silica nanoparticles; (C) silylated silica-octyl nanoparticles; (D) silylated silica-anthracene nanoparticles; the dash line stands for the interfacial tension between water and heptane + toluene mixture (volume ratio 50:50), measured at 23°C and atmospheric pressure.

Figure 4.8(A) shows the equilibrium interfacial tension between silica nanoparticle suspension and NaCl, and silica nanoparticle suspension and $CaCl_2$ solutions at different salinity. The equilibrium interfacial tension at low concentrations (1 mM and 10 Mm) is not so significant, for both types of salts. There is a substantial impact at 100mM. The $CaCl_2$ has a stronger impact on the nanoparticle adsorption process than NaCl. The reason is that each Ca^{2+} ion carries two unit charges, while Na^{+} ion carries only one unit charge, which makes Ca^{2+} ion more effective at neutralizing the surface charge of silica

nanoparticles. As mentioned in previous section, the neutralization of particle surface charge results in a higher surface excess concentration on the interface, which leads to the reduction in interfacial tension. Figure 4.8(B) shows the equilibrium interfacial tension between silylated silica nanoparticle suspension and NaCl or $CaCl_2$ solutions. The two curves of NaCl and $CaCl_2$ are quite close which indicates that the effect of Na^+ and Ca^{2+} ions is similar. No matter what salt is in the solution, the equilibrium interfacial tension when the concentration is 10 mM is around 37.25 mN/m and 36.50 mN/m for 100 mM. The change in equilibrium in interfacial tension is not obvious even though the salt concentration changed 10 times, which could indicate that higher salt concentration, might not be as effective as for silylated silica nanoparticle samples on lowering the equilibrium interfacial tension. Figure 4.8(C) shows the equilibrium interfacial tension between silylated silica-octyl nanoparticle suspension and NaCl or $CaCl_2$ solutions. When the concentration is 10 mM and 100 mM, the equilibrium interfacial tension between NP suspension and $CaCl_2$ solution is lower than with NaCl solution. The effect of Ca^{2+} ions is stronger under higher concentration. No matter what salt is in the solution, the equilibrium interfacial tension when the concentration is 10 mM is around 35.5 mN/m and 35.0mN/m for 100 mM. The change in equilibrium in interfacial tension is not obvious even though the salt concentration changed 10 times, which could indicate that higher salt concentration might not be as effective as for silylated silica-octyl nanoparticle samples on lowering the equilibrium interfacial tension. Figure 4.8(D) shows the equilibrium interfacial tension between silylated silica-anthracene nanoparticle suspension and NaCl or $CaCl_2$ solutions. Sodium ions are more effective at neutralizing the surface charge especially when the salt concentration is low and the detailed reason is

discussed before. As the silylated silica-anthracene nanoparticles turn into aggregates, the surface charge that can be neutralized is reduced considering that hydrated ions may not be able to get into the aggregates. When the salt concentration is higher, like 100 mM, the surface charge of nanoparticle aggregates could be fully neutralized. Thus, when the concentration is 100 mM, two ions are almost as effective as each other.

Ionic strength is introduced here to describe the activity coefficients of electrolyte. When the concentration of NaCl and $CaCl_2$ solution is the same, on a mole/L basis, the ionic strength of $CaCl_2$ is 3 times of the ionic strength of NaCl, which is possible that the $CaCl_2$ has a stronger effect with bare silica nanoparticles.

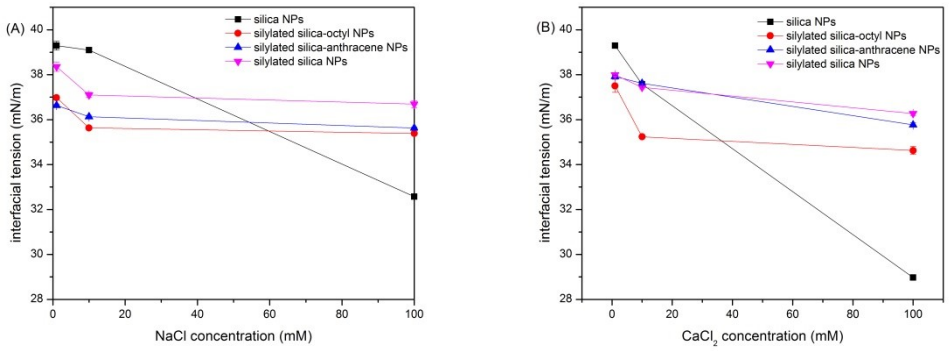

Figure 4.9 (A) Na^+ ions effect (B) Ca^{2+} ions effect on equilibrium interfacial tension between water and silica nanoparticles in heptane + toluene. The dash line stands for the interfacial tension between water and heptane + toluene mixture (volume ratio 50:50), measured at 23°C and atmospheric pressure.

Figure 4.9(A) shows the effect of sodium ions on all the four types of silica nanoparticle samples. From the graph, it is clear that when the concentration of NaCl is low, the effect

of salt on lowering the interfacial tension is very limited and can be neglected for silica nanoparticle dispersions while at 100 mM, the equilibrium interfacial tension drops to 32.5 mN/m which is the lowest value that can be reached. For the other three functionalized silica nanoparticles, higher salinity (100 mM) does not have much impact as for silica nanoparticles. Sodium chloride has the least effect for silylated silica nanoparticles. The possible reason is that the functional group (trimethylsilane -$Si(CH_3)_3$) which is smaller compared with octyl and anthracene functional groups. Thus the steric repulsion which can prevent the nanoparticles from aggregation between silylated silica nanoparticles is weaker than silylated silica-octyl nanoparticles. In addition, the surface properties of silylated silica nanoparticles make it easier to neutralize the surface charge on them. Overall, both factors can cause silylated silica nanoparticles to aggregate and to be less effective. The concentration of sodium ions can affect the adsorption process of silylated silica and silylated silica-octyl nanoparticles at lower concentration (from 1 mM to 10 mM). However, when the sodium ion concentration changes from 10 mM to 100 mM, the impact of concentration on the adsorption is not as strong as from 1 mM to 10 mM. The possible reason is that most surface charge on nanoparticles is already neutralized when the concentration is 10 mM. Thus, further increase in salt concentration does not have much impact.

Figure 4.9(B) shows the effect of calcium ions on all the four types of silica nanoparticle samples. As for sodium ions, when the concentration of $CaCl_2$ is low, the effect of salt on lowering the interfacial tension is quite small for silica nanoparticles dispersions. However, when the concentration reaches 100 mM, the equilibrium interfacial tension

drops to 29 mN/m which is the lowest value that can be achieved among all of the cases studied. As for sodium ions, higher salinity (100 mM) does not have much impact on the functionalized silica nanoparticles as for silica nanoparticles. Calcium chloride has least effect for both silylated silica and silylated silica-anthracene nanoparticles. The effect of concentration of calcium ions is quite limited for silylated silica and silylated silica-anthracene nanoparticles. But the concentration of calcium ions influence the adsorption when the concentration changes from 1 mM to 10 mM because most surface charge are neutralized at 10 mM.

Figure 4.10 shows normalized kinetics for bare silica nanoparticle adsorption on the water/heptane+toluene mixture interface. where Q is:

$$Q = \frac{\gamma - \gamma_e}{\gamma_0 - \gamma_e} \tag{4.1}$$

γ is the IFT at some time, γ_e is the steady state IFT, γ_0 is the initial IFT defined as the average IFT of first 100 measurements.

From Figure 4.10 (A) and (B), it is clear that when the salt concentration is 100 mM, the time needed for the system to reach γ_e is shorter for both NaCl and $CaCl_2$, which indicates that the adsorption process is faster under 100 mM. However, at concentration of 1 mM and 10 mM, the curves are very close to each other for the same salt solution, which indicates that lower salt concentration has limited impact on the particle adsorption process. For the other three functionalized silica nanoparticle: silylated silica, silylated silica-octyl and silylated silica-anthracene nanoparticles, the differences amongadsorption

process at different salt concentrations are not as pronounced as for bare silica nanoparticles.

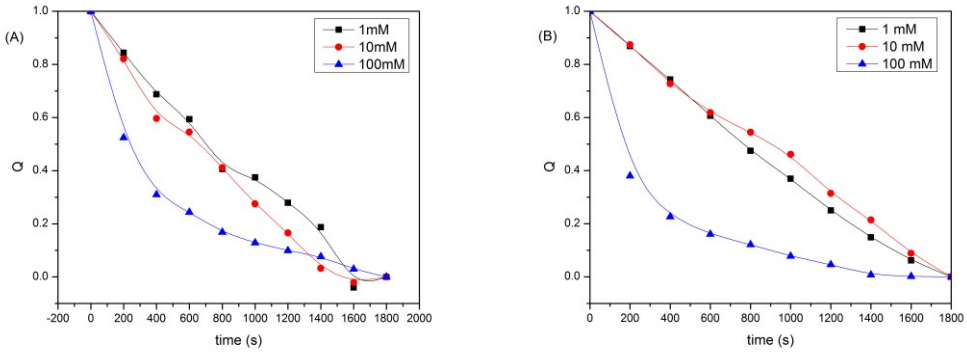

Figure 4.10 Normalized bare silica nanoparticle adsorption on the aqueous solution/heptane+toluene mixture; (A) with NaCl solution; (B) with $CaCl_2$ solution.

4.4 Summary

Silica nanoparticles whether they are functionalized or not, have measurable but limited impacts on dynamic and steady state interfacial tension values between Toluene and toluene + heptane mixture (volume ratio 50:50)and water irrespective of water pH and salt content. The cores of silica nanoparticles dominate their surface behaviors. Silica nanoparticles are not good emulsion stabilizers for the cases studied. Neutral pH is favored for oil in water emulsion breakage. Acidic and especially alkaline environments are not favored for emulsion breakage because the interfacial tension is lower.

The effect of sodium chloride and calcium chloride salts on the IFT of water and silica nanoparticles in heptane + toluene (volume ratio 50:50)suspensions varies with salt

concentration and salt type but the effect is a secondary one and is similar for all of the functionalized silica nanoparticles. Higher salt concentration in the aqueous phase decreases the IFT between hydrocarbon and the water phases. This probably arises from the similarity of the surface charge neutralization by the ions which allows for similar excess surface concentrations at saturation. For bare silica nanoparticles, more active surface sites are available and IFT continues to be impacted at higher salt concentrations. However, more work is needed on this point.

Functional groups on the silica nanoparticle surfaces also induce aggregation where none is observed for unmodified silica nanoparticles under higher particle concentration.

4.5 References

(1) Kahaniani, Y.; Shaw, J. M. Characterization and Shear Rheology of Silica Nanoparticles Functionalized with Alkyl and Alkyl-Aromatic Ligands. Internal Report 2014, 13.

(2) D.R. Burgess "Thermochemical Data" in NIST Chemistry Webbook, NIST Standard Reference Database Number 69, 2017.

(3)Binks, B. P. Particles as Surfactants—similarities and Differences. *Current opinion in colloid & interface science* **2002***, 7*, 21-41.

(4) Adamczyk, Z.; Siwek, B.; Zembala, M. Reversible and Irreversible Adsorption of Particles on Homogeneous Surfaces. Colloids and Surfaces 1992, 62, 119-130.

(5) Hu, C.; Garcia, N. C.; Xu, R.; Cao, T.; Yen, A.; Garner, S. A.; Macias, J. M.; Joshi, N.; Hartman, R. L. Interfacial Properties of Asphaltenes at the Heptol–Brine Interface. Energy Fuels 2015, 30, 80-87.

(6) Aveyard, R.; Saleem, S. M. Interfacial Tensions at Alkane-Aqueous Electrolyte Interfaces. Journal of the Chemical Society, Faraday Transactions 1: Physical Chemistry in Condensed Phases 1976, 72, 1609-1617.

(7) Cai, B.; Yang, J.; Guo, T. Interfacial Tension of Hydrocarbon Water/Brine Systems Under High Pressure. Journal of chemical & engineering data 1996, 41, 493-496.

(8) Israelachvili, J. N. In Intermolecular and surface forces; Academic press: 2015; 367.

(9) Martinez, C. R.; Iverson, B. L. Rethinking the Term “pi-Stacking”. Chemical Science 2012, 3, 2191-2201.

Chapter 5 Conclusions and future work

5.1 Conclusions

Four types of silica nanoparticles were used to mimic clay and oil contaminated clay particles on oil/water interfaces. All four silica nanoparticles were characterized by FTIR. One particle type is bare silica and three are functionalized silica nanoparticles including silylated silica, silylated silica-octyl and silylated silica-anthracene nanoparticles. The impacts of these organic ligands on nanoparticle surfaces on IFT values at toluene/heptane (volume ratio 50:50) + water (salt, pH) were illustrated and in most cases their behaviours were discriminated.

More specifically, the nanoparticle concentrations studied in this work were 100 mg/L, 300 mg/L and 500 mg/L. Nanoparticles have a small but measurable impact on IFT at neutral pH. Silica and silylated-anthracene nanoparticles reduced interfacial tension with increasing concentration in this range. Silylated silica and silylated silica-octyl nanoparticles aggregated and were less effective at reducing the interfacial tension at neutral pH.

Six values of pH were chosen to explore the effect of pH from 2 to 12. The cross plot between equilibrium interfacial tension and pH is bell-shaped. The minimum reduction in interfacial tension occurs around neutral pH. In acidic and especially in alkaline environments IFT is reduced but the impact is of secondary importance for all four particle types at 300 mg/L.

Impacts of NaCl and $CaCl_2$ on IFT values were studied at 1 mM, 10 mM and 100 mM in water at neutral pH. The extent of the reduction in IFT values varied with cation and salt concentration and the surface properties of the silica nanoparticles at 300mg/L but showed a similar trend - interfacial tension decreases with increasing salinity. The effect was greatest for bare silica nanoparticles and less for silylated silica, silylated silica-octyl and silylated silica-anthracene nanoparticles.

5.2 Future Work

1. Additional functional groups relevant to hydrocarbon production and environmental applications are worthy of study. Examples include thiol and carboxyl groups.

2. The influence of temperature and pressure on outcomes arising in this work merit further study. The impact of temperature can be investigated with heated environmental cell which can control the temperature of the system. The impact of pressure can be studied with high pressure chamber.

3. Janus particles (half of each particle with one of two ligands attached) or particles including two randomly distributed but different functional groups or mixtures of particles with different ligands also merit investigation.

4. Characterize aggregates of particles aggregates on interfaces, using a confocal microscope and/or a fluorescence measurement method.

Appendix: Supplementary data

1) DLS measurements for silylated silica-anthracene nanoparticles in toluene suspension at 500 mg/L.

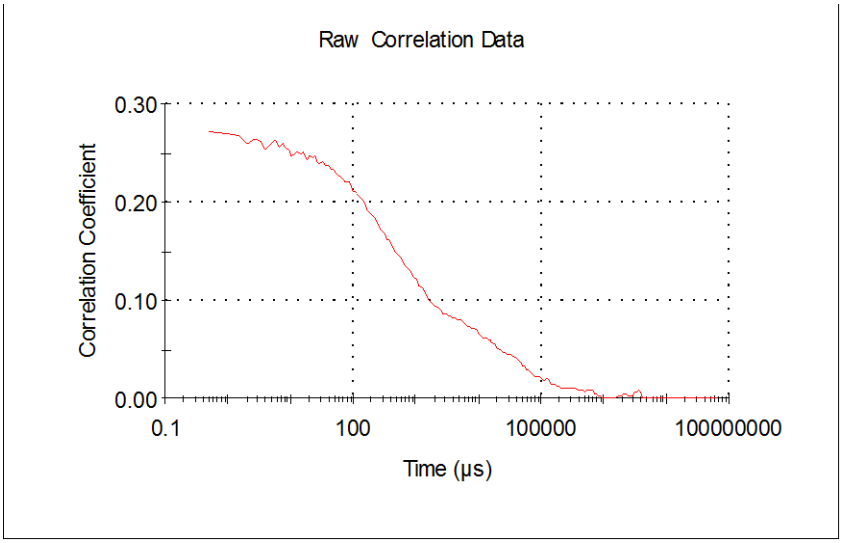

Figure 1 Raw correlation data.

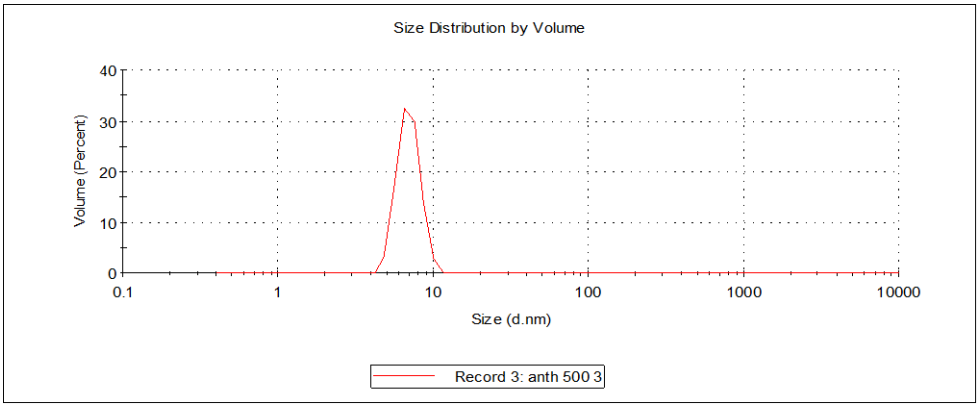

Figure 2 Size distribution by volume.

Sample Name:	anth 500 3		
SOP Name:	mansettings.nano		
File Name:	anth 500 size.dts	**Dispersant Name:**	Toluene
Record Number:	3	**Dispersant RI:**	1.496
Material RI:	1.46	**Viscosity (cP):**	0.5762
Material Absorbtion:	0.010	**Measurement Date and Time:**	Wednesday, July 13, 2016 2:27:00

Temperature (°C):	22.0	**Duration Used (s):**	60
Count Rate (kcps):	46.6	**Measurement Position (mm):**	4.65
Cell Description:	Glass cuvette with square aperture	**Attenuator:**	8

			Size (d.nm):	**% Intensity:**	**St Dev (d.nm):**
Z-Average (d.nm):	1183	**Peak 1:**	214.4	89.7	40.05
PdI:	0.759	**Peak 2:**	7.321	10.3	0.9185
Intercept:	0.498	**Peak 3:**	0.000	0.0	0.000

Result quality : Refer to quality report

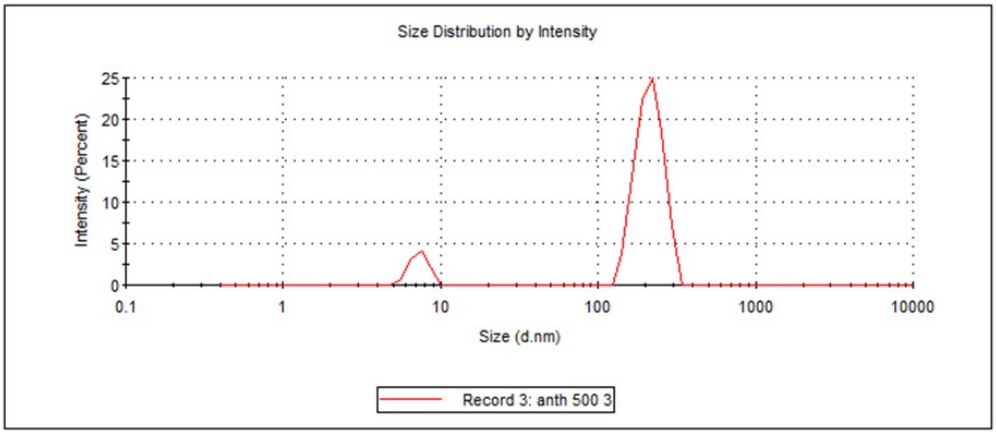

Figure 3 Information on size distribution and size distribution by intensity.

Bibliography

Golby, S.; Ceri, H.; Gieg, L.,M.; Chatterjee, I.; Marques, L.,L.R.; Turner, R.,J. Evaluation of Microbial Biofilm Communities from an Alberta Oil Sands Tailings Pond. FEMS Microbiology Ecology 2012, 79, 240-250.

Masliyah, J.; Czarnecki, J.; Xu, Z. Handbook on Theory and Practice of Bitumen Recovery from Athabasca Oil Sands. Theoretical Basis 2011, 1.

Mikula, R. J.; MuÑoz, V. A.; Omotoso, O. Centrifugation Options for Production of Dry Stackable Tailings in Surface Mined Oil Sands Tailings Management. Journal of Canadian Petroleum Technology 2009, 48, 19-23.

Quagraine, E. K.; Peterson, H. G.; Headley, J. V. In Situ Bioremediation of Naphthenic Acids Contaminated Tailing Pond Waters in the Athabasca Oil Sands Region-Demonstrated Field Studies and Plausible Options: A Review. Journal of Environmental Science and Health, Part A 2005, 40, 685-722.

Song, B.; Springer, J. Determination of Interfacial Tension from the Profile of a Pendant Drop using Computer-Aided Image Processing. Journal of Colloid and Interface Science 1996, 184, 64-76.

Tariq Siddique; Phillip M Fedorak; Michael D MacKinnon; Julia M Foght Metabolism of BTEX and Naphtha Compounds to Methane in Oil Sands Tailings. Environmental science & technology 2007, 41, 2350-2356.

OIL SANDS MAGAZINE TAILINGS PONDS 101.

http://www.oilsandsmagazine.com/technical/mining/tailings-ponds.

Song, B.; Springer, J. Determination of Interfacial Tension from the Profile of a Pendant Drop using Computer-Aided Image Processing. Journal of Colloid and Interface Science 1996, 184, 64-76.

Hunter, R. J. In Foundations of Colloid Science; Oxford University Press: New York, 2001; 25-28.

Madejová, J. FTIR Techniques in Clay Mineral Studies. Vibrational Spectroscopy 2003, 31, 1-10.

Henderson, D. Recent Progress in the Theory of the Electric Double Layer. Prog Surf Sci 1983, 13, 197-224.

Hermansson, M. The DLVO Theory in Microbial Adhesion. Colloids and Surfaces B: Biointerfaces 1999, 14, 105-119.

Gregory, J.; O'Melia, C. R. Fundamentals of Flocculation. Crit. Rev. Environ. Sci. Technol. 1989, 19, 185-230.

Chan, M. C. W. A Novel Flocculant for Enhanced Dewatering of Oil Sands Tailings, ProQuest Dissertations Publishing, 2011.

World Wildlife Fund In Tailings, a lasting oil sands legacy; World Wildlife Fund Canada: Toronto, Ont., 2010; 40.

Suncor Energy Inc. SUNCOR ENERGY INC. Oil Sands

DDA Plan Prepared in accordance with Directive 074 – Appendix C, 2010.

Gibbs, J. W. In The Scientific Papers of J. Willard Gibbs; Dover: New York, 1961; Vol. 1, pp 55-371.

KRUSS Interfacial tension. https://www.kruss.de/services/education-theory/glossary/interfacial-tension/.

J. G. Calvert Glossary of Atmospheric Chemistry Terms (Recommendations 1990). Pure and Applied Chemistry 1990, 62, 2167-2219.

Rosen, M. J.; Kunjappu, J. T. In Surfactants and Interfacial Phenomena; John Wiley & Sons: Hoboken, 2012; pp 618.

Foo, K. Y.; Hameed, B. H. Insights into the Modeling of Adsorption Isotherm Systems. Chemical Engineering Journal 2010, 156, 2-10.

STRASSNER, J. E. Effect of pH on Interfacial Films and Stability of Crude Oil-Water Emulsions. Journal of Petroleum Technology 1968, 20, 303-312.

Havre, T. E.; Sjöblom, J.; Vindstad, J. E. Oil/Water-partitioning and Interfacial Behavior of Naphthenic Acids. J. Dispersion Sci. Technol. 2003, 24, 789-801.

Speight, J. G. In Lange's handbook of chemistry; McGraw-Hill New York: 2005; Vol. 1.

Acevedo, S.; Escobar, G.; Gutiérrez, L.; Rivas, H. Isolation and Characterization of Natural Surfactants from Extra Heavy Crude Oils, Asphaltenes and Maltenes. Interpretation of their Interfacial Tension-pH Behaviour in Terms of Ion Pair Formation. Fuel 1992, 71, 619-623.

Poteau, S.; Argillier, J.; Langevin, D.; Pincet, F.; Perez, E. Influence of pH on Stability and Dynamic Properties of Asphaltenes and Other Amphiphilic Molecules at the Oil−Water Interface. Energy & Fuels 2005, 19, 1337-1341.

Denoyel, R.; Rouquerol, J. Thermodynamic (Including Microcalorimetry) Study of the Adsorption of Nonionic and Anionic Surfactants Onto Silica, Kaolin, and Alumina. J. Colloid Interface Sci. 1991, 143, 555-572.

Mackay, D.; Hossain, K. Interfacial Tensions of Oil, Water, Chemical Dispersant Systems. The Canadian Journal of Chemical Engineering 1982, 60, 546-550.

Cai, B.; Yang, J.; Guo, T. Interfacial Tension of Hydrocarbon Water/Brine Systems Under High Pressure. Journal of chemical & engineering data 1996, 41, 493-496.

Lashkarbolooki, M.; Riazi, M.; Ayatollahi, S.; Hezave, A. Z. Synergy Effects of Ions, Resin, and Asphaltene on Interfacial Tension of Acidic Crude Oil and Low–high Salinity Brines. Fuel 2016, 165, 75-85.

Schott, H.; Royce, A. E.; Han, S. K. Effect of Inorganic Additives on Solutions of Nonionic Surfactants: VII. Cloud Point Shift Values of Individual Ions. J. Colloid Interface Sci. 1984, 98, 196-201.

Somasundaran, P. In Encyclopedia of surface and colloid science; CRC Press: Boca Raton, Fla. [u.a.], 2016; 54-68.

Bai, J.; Fan, W.; Nan, G.; Li, S.; Yu, B. Influence of Interaction between Heavy Oil Components and Petroleum Sulfonate on the Oil–water Interfacial Tension. J. Dispersion Sci. Technol. 2010, 31, 551-556.

Jennings, H. Y. The Effect of Temperature and Pressure on the Interfacial Tension of Benzene-Water and Normal Decane-Water. Journal of Colloid and Interface Science 1967, 24, 323-329.

Sarikhani, K.; Jeddi, K.; Thompson, R. B.; Park, C. B.; Chen, P. Effect of Pressure and Temperature on Interfacial Tension of Poly Lactic Acid Melt in Supercritical Carbon Dioxide. Thermochimica Acta 2015, 609, 1-6.

Jennings Jr, H. Y.; Newman, G. H. The Effect of Temperature and Pressure on the Interfacial Tension of Water Against Methane-Normal Decane Mixtures. Society of Petroleum Engineers Journal 1971, 11, 171-175.

Hughey, C. A.; Rodgers, R. P.; Marshall, A. G. Resolution of 11 000 Compositionally Distinct Components in a Single Electrospray Ionization Fourier Transform Ion Cyclotron Resonance Mass Spectrum of Crude Oil. Anal. Chem. 2002, 74, 4145-4149.

Simanzhenkov, V.; Idem, R. In Crude oil chemistry; Marcel Dekker: New York, 2003; pp 409.

Bazyleva, A., Becerra, M., Stratiychuk-Dear, D., and Shaw, J. M., Phase behavior of Safaniya vacuum residue. Fluid Phase Equilibria, 2014. 380(0): p. 28-38.

Zhao, B.; Shaw, J. M. Composition and Size Distribution of Coherent Nanostructures in Athabasca Bitumen and Maya Crude Oil. Energy & Fuels 2007, 21, 2795-2804.

Eyssautier, J. l., Espinat, D., Gummel, J. r. m., Levitz, P., Becerra, M., Shaw, J., and Barré, L., Mesoscale Organization in a Physically Separated Vacuum Residue: Comparison to Asphaltenes in a Simple Solvent. Energy & Fuels, 2012. 26(5): p. 2680-2687.

Spiecker, P. M.; Gawrys, K. L.; Trail, C. B.; Kilpatrick, P. K. Effects of Petroleum Resins on Asphaltene Aggregation and Water-in-Oil Emulsion Formation. Colloids Surf. Physicochem. Eng. Aspects 2003, 220, 9-27.

Gray, M. R. In Upgrading Oilsands Bitumen and Heavy Oil; Pica Pica Press: Edmonton, 2015; 2-6.

Tsamantakis, C.; Masliyah, J.; Yeung, A.; Gentzis, T. Investigation of the Interfacial Properties of Water-in-Diluted-Bitumen Emulsions using Micropipette Techniques. J. Colloid Interface Sci. 2005, 284, 176-183.

Yarranton, H. W.; Hussein, H.; Masliyah, J. H. Water-in-Hydrocarbon Emulsions Stabilized by Asphaltenes at Low Concentrations. J. Colloid Interface Sci. 2000, 228, 52-63.

Huang, C.; Notten, A.; Rasters, N. Nanoscience and Technology Publications and Patents: A Review of Social Science Studies and Search Strategies. The Journal of Technology Transfer 2011, 36, 145-172.

Taylor, R.; Coulombe, S.; Otanicar, T.; Phelan, P.; Gunawan, A.; Lv, W.; Rosengarten, G.; Prasher, R.; Tyagi, H. Small Particles, Big Impacts: A Review of the Diverse Applications of Nanofluids. J. Appl. Phys. 2013, 113, 1.

Schiffelers, R. M.; Ansari, A.; Xu, J.; Zhou, Q.; Tang, Q.; Storm, G.; Molema, G.; Lu, P. Y.; Scaria, P. V.; Woodle, M. C. Cancer siRNA Therapy by Tumor Selective Delivery with Ligand-Targeted Sterically Stabilized Nanoparticle. Nucleic Acids Res. 2004, 32, e149.

Mrup, S.; Hansen, M. F.; Frandsen, C. Magnetic Interactions between Nanoparticles. Beilstein journal of nanotechnology 2010, 1, 182.

Zhong, C.; Maye, M. M. Core–shell Assembled Nanoparticles as Catalysts. Adv Mater 2001, 13, 1507-1511.

Calero, P.; Martínez-Máñez, R.; Sancenón, F.; Soto, J. Synthesis, Characterisation and Optical Properties of Silica Nanoparticles Coated with Anthracene Fluorophore and Thiourea Hydrogen-Bonding Subunits. European Journal of Inorganic Chemistry 2008, 2008, 5649-5658.

Montalti, M.; Prodi, L.; Zaccheroni, N.; Falini, G. Solvent-Induced Modulation of Collective Photophysical Processes in Fluorescent Silica Nanoparticles. J. Am. Chem. Soc. 2002, 124, 13540-13546.

Badiei, A.; Bonneviot, L.; Crowther, N.; Ziarani, G. M. Surface Tailoring Control in Micelle Templated Silica. Journal of organometallic chemistry 2006, 691, 5911-5919.

Kahaniani, Y.; Shaw, J. M. Characterization and Shear Rheology of Silica Nanoparticles Functionalized with Alkyl and Alkyl-Aromatic Ligands. Internal Report 2014, 13.

Cerveny, S.; Schwartz, G. A.; Otegui, J.; Colmenero, J.; Loichen, J.; Westermann, S. Dielectric Study of Hydration Water in Silica Nanoparticles. The Journal of Physical Chemistry C 2012, 116, 24340-24349.

PragoLab In pH Measurement Handbook Thermo Scientific, Inc.: 2017;2-4.

Kumar, B. Effect of Salinity on the Interfacial Tension of Model and Crude Oil Systems, University of Calgary, 2012.

Carl Clegg Ramé-Hart Goniometer Model 250 Pictures. https://www.flickr.com/photos/51015268@N07/sets/72157634050986433/.

Jian, C.; Poopari, M. R.; Liu, Q.; Zerpa, N.; Zeng, H.; Tang, T. Reduction of Water/Oil Interfacial Tension by Model Asphaltenes: The Governing Role of Surface Concentration. The Journal of Physical Chemistry B 2016, 120, 5646-5654.

Berne, B. J.; Pecora, R. In Dynamic light scattering: with applications to chemistry, biology, and physics; Courier Corporation: 2000; 10-45.

Washington, C. In Particle Size Analysis In Pharmaceutics And Other Industries: Theory And Practice: Theory And Practice; CRC Press: 2005;101-106 .

Griffiths, P. R.; De Haseth, J. A. In Fourier transform infrared spectrometry; John Wiley & Sons: 2007; Vol. 171.

Saptari, V. In Fourier transform spectroscopy instrumentation engineering; SPIE press: 2004; Vol. 61.

Korb, A. R.; Dybwad, P.; Wadsworth, W.; Salisbury, J. W. Portable Fourier Transform Infrared Spectroradiometer for Field Measurements of Radiance and Emissivity. Appl. Opt. 1996, 35, 1679-1692.

Sanchonx Interferometer for FTIR. https://commons.wikimedia.org/wiki/File:FTIR_Interferometer.png.

Nanoparticles Functionalized with Alkyl and Alkyl-Aromatic Ligands. Internal Report 2014, 13.

D.R. Burgess "Thermochemical Data" in NIST Chemistry Webbook, NIST Standard Reference Database Number 69, 2017.

Binks, B. P. Particles as Surfactants—similarities and Differences. Current opinion in colloid & interface science 2002, 7, 21-41.

Adamczyk, Z.; Siwek, B.; Zembala, M. Reversible and Irreversible Adsorption of Particles on Homogeneous Surfaces. Colloids and Surfaces 1992, 62, 119-130.

Hu, C.; Garcia, N. C.; Xu, R.; Cao, T.; Yen, A.; Garner, S. A.; Macias, J. M.; Joshi, N.; Hartman, R. L. Interfacial Properties of Asphaltenes at the Heptol–Brine Interface. Energy Fuels 2015, 30, 80-87.

Aveyard, R.; Saleem, S. M. Interfacial Tensions at Alkane-Aqueous Electrolyte Interfaces. Journal of the Chemical Society, Faraday Transactions 1: Physical Chemistry in Condensed Phases 1976, 72, 1609-1617.

Cai, B.; Yang, J.; Guo, T. Interfacial Tension of Hydrocarbon Water/Brine Systems Under High Pressure. Journal of chemical & engineering data 1996, 41, 493-496.

Israelachvili, J. N. In Intermolecular and surface forces; Academic press: 2015; 367.

Martinez, C. R.; Iverson, B. L. Rethinking the Term “pi-Stacking”. Chemical Science 2012, 3, 2191-2201.